Running Title: A peroxisomal lipid-synthesizing enzyme promotes GC and Ab

B cell expression of the enzyme PexRAP, an intermediary in ether lipid biosynthesis, promotes antibody responses and germinal center size

Sung Hoon Cho[†@&*], Marissa A. Jones, Kaylor Meyer[†],

David M. Anderson[+], Sergei Chetyrkin[+], M. Wade Calcutt[+], Richard M. Caprioli[+],

Clay F. Semenkovich[~], Mark R. Boothby[†@&] *

Author affiliations †Department of Pathology-Microbiology-Immunology, [@]Vanderbilt Center for Immunobiology, and [&]Vanderbilt Institute for Infection, Inflammation, & Immunology, [+]Vanderbilt University Medical Center, Nashville, TN 37232; Mass Spectrometry Research Center and Department of Biochemistry, Vanderbilt University Medical School, and ^Cancer Biology Program, Vanderbilt University, Nashville TN 37212; [~] Division of Endocrinology. Metabolism & Lipid Research, Dept. of Medicine, Washington University, St. Louis MO 63110

* Correspondence: Sunghoon.Cho@vumc.org and Mark.Boothby@vumc.org

Dept. of Pathology, Microbiology & Immunology, Vanderbilt University Medical Center, AA-4214 MCN Building, 1161 21st Ave. S., Nashville, TN 37232-2363

ABSTRACT

The qualities of antibody (Ab) responses provided by B lymphocytes and their plasma cell (PC) descendants are crucial facets of responses to vaccines and microbes. Metabolic processes and products regulate aspects of B cell proliferation and differentiation into germinal center (GC) and PC states as well as Ab diversification. However, there is little information about lymphoid cell-intrinsic functions of enzymes that mediate ether lipid biosynthesis, including a major class of membrane phospholipids. Imaging mass spectrometry (IMS) results had indicated that concentrations of a number of these phospholipids were substantially enhanced in GC compared to the background average in spleens. However, it was not clear if biosynthesis in B cells was a basis for this finding, or whether such cell-intrinsic biosynthesis contributes to B cell physiology or Ab responses. Ether lipid biosynthesis can involve the enzyme PexRAP, the product of the *Dhrs7b* gene. Using combinations of IMS and immunization experiments in mouse models with inducible *Dhrs7b* loss-of-function, we now show that B lineage-intrinsic expression of PexRAP promotes the magnitude and affinity maturation of a serological response. Moreover, the data revealed a *Dhrs7b*-dependent increase in ether phospholipids in primary follicles with a more prominent increase in GC. Mechanistically, PexRAP impacted B cell proliferation via enhanced survival associated with controlling levels of ROS and membrane peroxidation. These findings reveal a vital role of this peroxisomal enzyme in B cell homeostasis and the physiology of humoral immunity.

Abbreviations used:

Ag, antigen; Ab, antibody; WT, wildtype; KO, knockout; MZB, marginal zone B cell; FoB, follicular B cell; PC, plasma cell; Ig, immunoglobulin; GC, germinal center; ETC, electron transport chain; ROS, reactive oxygen species; mtROS, mitochondrial ROS; FAO, fatty acid oxidation; EL, ether lipid(s); 2D, 2-dimensional; MALDI, matrix-assisted laser desorption/ionization; IMS, imaging mass spectrometry; ER, Endoplasmic Reticulum; PexRAP, Peroxisomal Reductase Activating PPARγ; DHAP, dihydroxyacetonephosphate; G3P, glycerol-3-phosphate; CTV, CellTrace Violet; SRBC, sheep red blood corpuscule; TCR, T cell receptor; CD, Cluster of differentiation; AID, Activation-induced deaminase; GFP, Green fluorescent protein; NP-OVA, 3-Nitrophenylacetyl (NP)-ovalbumin (OVA); ASCs, Ab-secreting cells; CSR, class-switch recombination; MBC, memory B cell; NADPH, nicotinamide adenine dinucleotide phosphate; NAC, N-acetyl-L-cysteine; OCR, oxygen consumption rate; ECAR, extracellular acidification rate; RCDP, rhizomelic chondrodysplasia punctata; FAS, fatty acid synthase; Tmx, tamoxifen; 4OHT, 4-hydroxytamoxifen; PUFA, poly-unsaturated fatty acids; 2-DG, 2-deoxyglucose; FCCP, carbonyl cyanide 4-phenylhydrazone; BSA, bovine serum albumin; PSA, porcine serum albumin; H2DCFDA, dichlorodihydrofluorescein diacetate; ELISA, enzyme-linked immunosorbent assay; ELISpot, enzyme-linked immunosorbent spot; DHA, dihydroxyacetophenone; DAN, 1,5-diaminonaphthalene; timsTOF, trapped ion mobility spectrometry time-of-flight; SDS-PAGE, sodium dodecyl-sulfate polyacrylamide gel electrophoresis; SEM, standard error of means.

INTRODUCTION

The qualities and concentrations of antigen (Ag)-specific antibodies (Ab) are key elements of immunity and the pathophysiology of diverse conditions involving inflammation (1-3). Ab are secreted by cells in the B lymphocyte lineage, but the exact sources are diverse (4-7). Many derive from a subset termed B1 B cells, which are thought to having characteristics of innate responses (4, 5), but progeny of follicular and marginal zone B cells (FoB and MZB, respectively) can differentiate into Ab-secreting plasma cells (PC) after activation and proliferation (6-8). In addition to Ab concentrations and affinity for Ag, the efficacy of pathogen clearance can depend on the isotype to which B lymphocytes may transfer the Ag-combining variable region from an IgM heavy chain constant region to a new immunoglobulin (Ig) heavy chain (9-12). Importantly, the affinities of serum Ab for target Ag can increase over time after an immune exposure, especially after recurrent encounter(s) (8, 9, 13, 14).

Many sources and forms of Ab can be protective, though in several autoimmune diseases these molecules and the somatic mutations that diversify an initial BCR repertoire drive pathology (15, 16). A micro-anatomic structure termed the secondary follicle or germinal center (GC) provides one mechanism to increase spectrum of Ab affinities over time and repeated Ag exposure (17-19). Although diversification can, like PC production, occur independent from GC, results with different forms of vaccination support the practical importance of T cell help (20) and of this micro-anatomic process (21). Current evidence holds that most Ig class-switching is executed before GC entry of proliferating B cells (22). GC reactions are initiated after B cells in a primary lymphoid follicle encounter Ag, migrate to interact with activated helper T cells after extensive proliferation (23). GC formation, size, and function depend on factors that include both the efficiency of population growth for B cells in a phase before they enter and take on characteristics of GC B cells, and on homeostatic and differentiative processes while in the secondary follicle [reviewed in (24)]. Proliferation and selection end in development as Ab-secreting plasma cells or memory B cells [reviewed in (14, 18, 19)]. In line with a selection

28 process, substantial rates of B cell death have been measured in GC (25), so that determinants of
29 survival efficiency affect their outputs. As such, the qualities and quantities of Ab elicited by
30 immunization (or vaccination) depend on B cell proliferation and survival both prior to GC entry
31 as well as during GC reactions.
32
33 Accumulating evidence indicates that metabolic reprogramming and intermediary
34 metabolism play pivotal roles in survival, proliferation, differentiation and function in the pre-
35 immune populations that provide immune protection (26, 27), including B cells (28, 29). Among
36 core metabolic processes, several converge on oxidative metabolism fed by glycolytic generation
37 of pyruvate, anaplerotic use of amino acids such as glutamine, and fatty acid oxidation [reviewed
38 in (29, 30)]. Compared to resting populations such as naive B cells, rates of such metabolism in
39 B cells appear to be increased after activation, including in GC B cells [31-36; reviewed in (29)]
40 although in one case at a rate that may be less heightened in this specialized subset than after T-
41 independent B cell activation (33). Such increases support the generation of substrates for
42 anabolic processes in the dividing cell population and perhaps the energy demands thereof.
43
44 Mitochondria have been the focus of investigations exploring molecular mechanisms for
45 oxidative metabolism to generate energy and substrates in lymphocytes during immune
46 responses [reviewed in (37, 38)]. Oxidative phosphorylation in and dynamics of this organelle
47 appear to be important in determining rates of somatic hypermutation that characterize GC B cell
48 biology (33-35), albeit by a molecular mechanism that has not yet been identified. Use of the
49 Krebs TCA cycle to feed an electron transport chain (ETC) and efficient conversion of ADP to
50 ATP as a high-energy phosphate donor is among specialized functions of this highly dynamic
51 subcellular organelle. Along with other sources, mitochondria generate reactive oxygen species
52 (ROS) via the ETC at a rate determined by structural and biochemical features (39, 40). Rates of
53 ROS production, release, and resolution require regulation at multiple levels because these labile

54 species and their reactions with cellular molecules are important for both signaling and cell
55 proliferation but undermine cell function or survival when excessive.
56
57 B cells in most GC exhibit inadequacy of oxygen delivery relative to demands (31, 41-43).
58 Of note, genome-wide screening for genes that help cells adapt to hypoxia revealed a
59 requirement for peroxisomes and an ER enzyme involved in synthesizing plasmalogen ether
60 lipids (EL) (44). Using an unbiased lipidomic analysis that combined imaging mass spectrometry
61 (IMS) and techniques for identifying GC in sections of spleen from immunized mice, we had
62 found that after immunization, local concentrations of a subset of EL were heightened in GC
63 relative to other portions of the spleen (45). Ether phospholipids (EPL) have a fatty acid linked to
64 the glycerol backbone with an alkyl or a vinyl ether bond at the sn-1 position (46, 47). Synthesis
65 of ether phospholipids depends on the generation of precursors in peroxisomes and final
66 processing in the ER (48, 49). However, EL biosynthesis is prominent in the liver, and in theory
67 these species or their precursors might distribute to tissues from a primary site of biosynthesis or
68 from the diet (49-53). Thus, the finding that secondary follicles had greater densities of some -
69 but not all - ether phospholipids left several key questions unanswered – (1) Does the capacity to
70 synthesize and increase ether lipids in B cell follicles – primary or secondary (i.e., GC) - affect
71 antibody responses? (2) Are any of the EL dependent on B lineage-intrinsic metabolism to
72 generate precursors or final products? Moreover, there is debate whether EL or their plasmalogen
73 subset promote cell death or resistance, and whether inactivation of biosynthesis causes defects
74 in establishment or maintenance of hematopoietic cells (46, 53-55).
75
76 Peroxisomal Reductase Activating PPARγ (PexRAP, encoded by the *Dhrs7b* gene) catalyzes
77 the reduction of alkyl-dihydroxyacetonephosphate (DHAP) to 1-alkyl-G3P (46, 48, 56), which
78 then is transferred into endoplasmic reticulum (ER) and further metabolized to generate EL.
79 Recent work notes that this enzyme may substantially function in the ER in addition to the
80 peroxisome (56). Widespread inactivation of *Dhrs7b* in mature mice decreased hepatic

81 production of ether lipid species and reduced the population of erythrocytes and neutrophils (46).
82 Although questioned based on inborn errors of metabolism affecting other aspects of ether lipid
83 biosynthesis (54), this body of work indicated that PexRAP can be essential in some aspects of
84 ether lipid metabolism and may function in hematopoietic cells. Diverse functions of ether lipids
85 in general, and the plasmalogen subset in particular, have been proposed or supported by prior
86 work [reviewed in (57-61)]. The ether linkage may provide a sink for oxygen radicals - thereby
87 acting directly to resolve the reactivity and contribute to ROS homeostasis, although there is
88 debate as to the physiological impact of this chemical property (62). Whether or not this lipid
89 subset influences adaptive immunity or conventional lymphocyte lineages, however, is unclear.
90
91 Herein, we tested the hypotheses that (i) the ether lipid profiles in activated B cells depend
92 on their expression of the biosynthetic enzyme PexRAP [alternatively referred to as acyl/alkyl-
93 DHAP reductase (ADHAPR) (56)], and (ii) this enzyme promotes B cell physiology. To do so,
94 we combined conventional lipidomics, Imaging Mass Spectrometry (IMS), and immunization
95 experiments with genetic models in which loss-of-function for *Dhrs7b* is induced in adult mice.
96 We provide evidence that PexRAP impacts B cell proliferation via enhanced survival associated
97 with controlling levels of ROS and membrane peroxidation. The results also indicate that beyond
98 an impact on B cell homeostasis, GC are reduced in its absence, and the magnitude and affinity
99 maturation of a serological response depend on B cell expression of PexRAP. Taken together,
100 these finding support a function of B cell-intrinsic biosynthesis of ether lipids in B lymphocyte
101 homeostasis, the production of Ab, and in promoting GC reactions.
102
103
104
105

106 **RESULTS**
107

108 **PexRAP promotes homeostatic maintenance and proliferation of B cells.** By use of IMS, we
109 had reported that at least a dozen ether phospholipids - including plasmalogens - were enriched
110 in splenic germinal centers of immunized mice when compared to the rest of the tissue (45).
111 While previous work provided evidence that these lipid molecules were important for the
112 homeostasis of short-lived neutrophils (46), this effect was questioned based on inborn errors of
113 metabolism (54). Moreover, the impact of these molecules on adaptive immune cells or functions
114 is not known. Accordingly, we sought to test for effects of an intervention that interferes with a
115 key biosynthetic pathway used for endogenous synthesis of these molecules. To do so, we started
116 with analyses using induced loss-of-function for *Dhrs7b*$^{f/f}$ and the widely expressed *Rosa26-*
117 *CreER*^{T2} transgene (63, 64) used in (46), which reduced hepatic generation of a subset of ether
118 lipids and acts in all hematopoietic cells as well.
119

120 We modeled initial experiments on the published work with imaging mass spectrometry
121 (45). Mice were treated with tamoxifen using conditions less intense than a regimen shown to
122 have no effect on pre-immune splenic populations or B lineage (65, 66), immunized with SRBC
123 [akin to the analyses in (31, 36, 41, 45)], and analyzed 7 d after immunization (Fig. 1A).
124 Functional inactivation of *Dhrs7b* in T and B lymphocytes was confirmed by Western blot
125 analysis using anti-PexRAP Ab (Fig. 1B). The frequencies and numbers of CD19^{+} B220^{+} B cells
126 in *Dhrs7b*$^{f/f}$; *Rosa26-CreER*^{T2} - only a small minority of which would have been activated by the
127 immunization - were approximately 0.6 the values for controls (*Dhrs7b*$^{+/+}$ *Rosa26-CreER*^{T2},
128 i.e., wild-type locus) (Fig. 1C, D). In contrast to B cell populations, TCRβ^{+} CD4^{+} T cells and
129 TCRβ^{+} CD4^{-} CD8 T cells were intact in tamoxifen-treated and SRBC-immunized *Dhrs7b*$^{f/f}$;
130 *Rosa26-CreER*^{T2} mice (Supplemental Fig. 1A-C). These results suggest that *Dhrs7b* is non-
131 redundantly required for fully functional B cell maintenance but indicate that the enzyme is
132 dispensable for the main populations of conventional T cells. In light of the earlier finding that a

133 subset of ether lipids was more prevalent in secondary follicles, we analyzed GC in these
134 samples. Microscopy and flow cytometry analyses after immunofluorescent staining found that
135 less GC B cells were present after immunization of *Dhrs7b*$^{f/f}$; *Rosa26-CreER*^{T2} mice, i.e., less
136 IgD^{-} CD95^{+} GL7^{+} (GC-phenotype) B cells (Fig. 1E-I; Supplemental Fig. 1D). Quantitation of the
137 immune fluorescence micrography with spleens from immunized mice revealed that the numbers
138 of GC per spleen were halved in *Dhrs7b*$^{\Delta/\Delta}$ mice compared with controls (Fig. 1I; Supplemental
139 Fig. 1E). The sizes of those GC that did form were substantially reduced as well (Fig. 1I;
140 Supplemental Fig. 1F). The lower number of B cells found in immunized mice - while a less
141 profound effect than the reduction in GC - tempers the result, and it was possible that the
142 function of helper CD4 T cells was impaired even their though numbers were not affected. While
143 not addressing whether or not B cells are part of the requirement for PexRAP in promoting GC,
144 these results indicate that *Dhrs7b* is necessary for a normal-sized geminal center response.
145
146 To determine if there are B lineage-specific functions of PexRAP, we used a conditionally
147 active Cre transgene that is expressed specifically in mature B cells (67). *Dhrs7b* f/f , *huCD20-*
148 *CreER*^{T2} mice and *huCD20-CreER*^{T2} were treated with tamoxifen to induce Cre-mediated
149 recombination of the floxed alleles after initial establishment of normal B cell populations (Fig.
150 2A). Western blot analyses showed an almost complete absence of PexRAP protein from B cells
151 purified from tamoxifen-treated *Dhrs7b*$^{f/f}$; *huCD20-CreER*^{T2} (hereinafter, *Dhrs7b*$^{\Delta/\Delta\text{-B}}$) mice
152 compared to similarly treated *huCD20*-CreER^{T2} controls (Fig. 2B). The enzyme encoded by this
153 gene catalyzes the synthesis of a lipid precursor to many - but not all - plasmalogens and other
154 ether phospholipids (46-48), and *Dhrs7b* deficiency impacted neutrophil survival (46). When we
155 tested if *Dhrs7b* inactivation affected the steady-state B cell population, the frequencies and total
156 numbers of CD19^{+} B220^{+} B cells in viable lymphocyte gates were about 20% lower in
157 tamoxifen-treated *Dhrs7b*$^{\Delta/\Delta\text{-B}}$ mice compared to tamoxifen-injected, *huCD20*-CreER^{T2},
158 *Dhrs7b*$^{+/+}$ controls (Fig. 2C). With loss-of-function after production of mature B cells, i.e.,
159 inactivation of *Dhrs7b* at ages over 6 wk, we observed balanced decreases in the numbers of

160 multiple subsets within the B lineage without evidence of selectivity among main sub-classes of
161 B cell (Supplemental Fig 1G-I). Thus, the frequencies of MZB and FOB amidst the smaller
162 population of splenic B cells in tamoxifen-treated *Dhrs7b*$^{f/f}$; *huCD20-CreER*^{T2} mice were similar
163 (Supplemental Fig 1H), and frequencies of B1 B cells in the peritoneal cavity also were
164 unaffected (Supplemental Fig 1I). Prior work documents normal frequencies and numbers of
165 developing and mature B cells under harsher conditions of tamoxifen-induced deletion with
166 CreER^{T2} (65). De novo B cell production rates are too low to yield the ~20% decrease observed
167 one week after gene disruption, and few splenic B cells are in cell cycle. Accordingly, we infer
168 that after maturation of a B cell, *Dhrs7b* promotes its survival, albeit to a modest degree.
169
170 B cell population growth can be impacted by increased cell death. To test if PexRAP affects
171 proliferation in vivo, *Dhrs7b*$^{\Delta/\Delta}$ B cells were stained with CellTrace Violet (CTV) and adoptively
172 transferred into B cell deficient μMT recipient mice. Strikingly fewer PexRAP-depleted B cells
173 were recovered (Fig. 2D), and the frequencies of *Dhrs7b*$^{\Delta/\Delta}$ B cells that were IgD^{-} (i.e., had been
174 activated) were half those of controls (Fig. 2E; supplemental Fig. S1J). As compared to control B
175 cells, CTV partitioning analyses suggested that division rates in vivo were modestly lower for
176 the *Dhrs7b*$^{\Delta/\Delta}$ B cells (Fig. 2F, G). Mitogen-stimulated *Dhrs7b*$^{\Delta/\Delta}$ B cells that proliferated in
177 culture exhibited substantially less robust division: frequencies of viable cells that had undergone
178 >3 divisions were halved in *Dhrs7b*$^{\Delta/\Delta}$ B cells) and yielded ~1/3 as large a progeny population
179 (Fig. 2G, H). Collectively, these data indicate that the *Dhrs7b* gene product supports homeostatic
180 maintenance of a quiescent (pre-immune) B cell population *in vivo* and effective proliferation of
181 B cells.
182
183 **B cell expression of PexRAP is required for achieving normally distributed concentrations**
184 **of ether phospholipids**. As noted, lipidomic analyses that used 2-dimensional image mass-
185 spectrometry (2D-IMS) discovered that local concentrations of a subset of ether lipids are
186 enriched in GC compared with the area outside of GC after immunization (45). To measure the

187 extent to which PexRAP expression within mature B cells can affect their lipid content and
188 composition, including their ether- and plasmalogen phospholipids, LC-MS-MS analyses were
189 performed with B cells directly isolated from spleens as well as those cultured after mitogenic
190 activation. These analyses showed substantial reductions in many ether phospholipids - as well
191 as lysophosphatidylethanolamines (LPE) generated by phospholipase cleavage of the R2 fatty
192 acid sidechain of an ether phospholipid - in PexRAP-deficient B cells (Fig. 3A, B; Supplemental
193 Fig. 2A, B). While beyond the scope of this work, this evidence suggests that generation of
194 potential signaling molecules via phospholipase(s) such as PLA2 may be reduced. Of note,
195 whereas differences were modest or absent in the naive population, the greatest impact of
196 PexRAP on quantitative amounts of phospholipids was found in the activated B cells, for which
197 tamoxifen treatment and CreERT2 made minimal differences (Supplemental Fig. 2C, D). Several
198 species, skewed towards those with the most detected ions, were at less than 1/5th the level of
199 non-deleted control B cells (Fig. 3C, D). There is no in vitro surrogate that faithfully represents
200 GC or the GC B cell, but collectively these data provide strong evidence that the capacity to
201 rapidly produce increased levels of many ether lipid molecules after lymphocyte activation
202 depends on a functional *Dhrs7b* gene in B cells. Although additional uptake or biosynthesis
203 pathways may add to the overall pool, as previously noted (46, 47) - and especially in resting B
204 cells that are out of cycle - the data indicate that *Dhrs7b* in B cells enhances cell-autonomous
205 biosynthesis. The straightforward inference is that PexRAP catalyzes the generation of ether lipid
206 precursors in amounts crucial for regulating the overall ether phospholipid pools, especially after
207 B cell activation.
208
209 Our earlier work (45) reported only ion mode features in negative mode and did not analyze
210 the primary follicle (the vast majority of which are resting B cells) relative to the extrafollicular
211 white pulp, red pulp, and GC. To investigate these issues and ultimately the requirement for
212 specific expression of PexRAP, we started with AID-GFP mice to enhance spatial localization.
213 These measurements confirmed that a substantial number of both positive and negatively

214 charged ions whose exact masses identified them as plasmalogens were substantially
215 concentrated in GC as compared to the rest of the B cell follicle (Table 1; Supplemental Fig. 3A,
216 B). Accordingly, we tested if the differential enrichment of any ether lipid species in primary or
217 secondary follicles depends on biosynthesis within a specific lymphoid lineage. Mice with
218 conditional mutations were tamoxifen-treated, immunized with SRBC, harvested seven days
219 thereafter, and analyzed by IMS (Fig. 4A, B). With deletion driven by the widely expressed
220 *Rosa26-CreER*^{T2} transgene, as in earlier work (46) and Fig. 1, substantial reductions of the GC
221 enrichment pattern were observed (Fig. 4C). For instance, two representative ions identified in
222 negative ion mode (i.e. *m/z* 752.5545 and *m/z* 776.5556) were again enriched in GC regions of
223 spleens from immunized WT mice. These features barely increased in splenic samples of
224 immunized *Dhrs7b*$^{\Delta/\Delta}$ (tamoxifen-injected *Dhrs7b*$^{f/f}$; *Rosa26-CreER*^{T2}) mice (Fig. 4C).
225
226 To determine if the levels of particular ether phospholipids in GC regions were affected by
227 PexRAP expression in B cells, *Dhrs7b*$^{f/f}$; *huCD20*-CreER^{T2} mice and *huCD20*-CreER^{T2} controls
228 were analyzed after tamoxifen injections followed by immunization, and compared to samples
229 from unimmunized mice. IMS using both positive and negative ion modes identified at least
230 eight ions - including *m/z* 752.5545, *m/z* 776.5556, and *m/z* 872.5749 - much more substantially
231 (~2-3-fold) concentrated in GC of immunized control mice (Fig. 4D, E; Table 2) than in the
232 primary follicle of unimmunized mice. Notably, these increased signals in secondary follicles
233 (GC) were reduced or almost completely eliminated in GCs of mice immunized after B cell-
234 specific PexRAP depletion (*Dhrs7b*$^{\Delta/\Delta\text{-B}}$) (Fig. 4D, E; Table 2; Supplemental Fig. 3C).
235 Collectively, these results indicate that *Dhrs7b* gene expression in activated B cells regulates the
236 spectrum of ether lipids in the micro-anatomic locale of a secondary follicle. Interestingly,
237 immunization also led to modest increases in the levels of some ether and conventional
238 phospholipids in the B cell-rich primary follicle regions (Table 2). This finding extends the
239 previous report (45), which focused on the relationship between the AID-GFP^{hi} region (i.e., GC)
240 and lipid features. Moreover, the absence of PexRAP blunted most of the immunization-induced

241 increases observed in the primary follicles. These findings and those of Fig. 3 suggest that there
242 are secondary consequences of *Dhrs7b* inactivation (e.g., some di-acyl phospholipids are
243 affected), but provide direct evidence that the enhancement of many ether phospholipid signals
244 in the GC depends on PexRAP in B cells.
245
246 **B cell-intrinsic role of *Dhrs7b* in Ab affinity and quantity.**
247 As key components of adaptive immunity, progeny of an activated B cell can differentiate
248 into Ab-secreting plasma cells (PC) or into GC B cells - whose physiology diversifies the affinity
249 for and breadth of antigen recognized by the original clone and improves properties of memory
250 [(14, 17-19, 68). PC that develop after a second encounter with antigen yield affinity maturation,
251 and the higher quality and proper quantity of Ag-specific Abs from plasma cells are integral to
252 humoral immune responses (68). An increasing body of evidence indicates that metabolic
253 reprogramming and intermediary metabolites modulate immune cell differentiation and function
254 (26-36). The observed B cell-intrinsic function of *Dhrs7b* in the accumulation of many ether
255 lipid species in both primary and secondary follicles prompted us to test the effect of B cell type-
256 restricted PexRAP depletion on GC responses and Ag-specific Ab production. Tamoxifen-
257 injected *Dhrs7b*$^{f/f}$; *huCD20-CreER*^{T2} and control mice were immunized with NP-ovalbumin (NP-
258 OVA), then boosted with NP-OVA to elicit affinity-matured Ab, and harvested 1 week thereafter
259 (Fig. 5A). Although PexRAP-deficient B cell numbers were reduced less than 20% a week after
260 starting gene inactivation prior to immunization (i.e., were over 0.8-fold those of controls) (Fig
261 2A-C), frequencies and numbers of IgD^{neg} B cells were halved in *Dhrs7b*$^{\Delta/\Delta\text{-B}}$ mice at harvest (4
262 wk after completion of the induced deletion) (Fig. 5B, C). Moreover, the GL7^{+} CD95^{+} fraction
263 of the B cell population in the dump / IgD^{neg} gate was substantially reduced (Fig. 5D), such that
264 numbers of GL7^{+} CD95^{+} GC B cells were dramatically decreased in *Dhrs7b*$^{\Delta/\Delta\text{-B}}$ mice (Fig. 5E).
265 Consistent with these findings, GC in *Dhrs7b*$^{\Delta/\Delta\text{-B}}$ mice were reduced after SRBC immunization,
266 with a modest change in the DZ/LZ ratio (Supplemental Fig. 4A, B).
267

268 Ab class-switch recombination (CSR) and affinity maturation can occur through
269 extrafollicular response, but the GC reaction significantly increases Ab diversification and high-
270 affinity Ab production, in part later in a primary response but also upon secondary exposure to
271 antigens (6, 8, 9, 17-19). ELISA on sera at 3 wk post-immunization (Fig. 6A-D), just before the
272 boost, showed that B cell-specific depletion of PexRAP prior to immunization reduced NP-
273 specific IgM and the switched isotype IgG1 (Fig. 6A, C). Of note, the capacity to generate high-
274 affinity Ab, detected with low valency NP2, was even more severely undermined than the overall
275 response - especially for IgG1 (Fig. 6B, D). A week after a second immunization, Ab-secreting
276 cells (ASCs) in the spleen (Fig. 6E) and circulating anti-NP IgM concentrations were diminished
277 in *Dhrs7b*$^{\Delta/\Delta-B}$ mice compared with controls that were *huCD20*-CreER^{T2}, *Dhrs7b*$^{+/+}$ treated with
278 tamoxifen in parallel to the mice with induced loss of PexRAP (Fig. 6F). The ratio of high-
279 affinity (NP2-binding) to all-affinity (NP20) IgM Ab also was substantially lower in *Dhrs7b*$^{\Delta/\Delta-B}$
280 mice (Fig. 6G), as were the serum levels of high-affinity IgG1 and IgG2c, class-switched
281 isotypes (Supplemental Fig. S4C, D). These data reinforce and extend the conclusion that the
282 expression of PexRAP in mature B cells is important for their physiology and function.
283
284 Consistent with *in vivo* results finding reduced Ag-specific ASCs in *Dhrs7b*$^{\Delta/\Delta-B}$ mice
285 compared with controls (Fig. 6E), the attenuated population of PexRAP-deficient B lineage cells
286 recovered after transfer into recipient mice (Fig. 2D) yielded lower frequencies of CD138^{+}
287 progeny (Fig. 6H, I) along with evidence of reduced activation [i.e., lower frequencies of IgD^{-}
288 progeny (Supplemental Fig. 1I). Mitogen-stimulated *Dhrs7b*$^{\Delta/\Delta}$ B cells also yielded lower
289 frequencies of CD138^{+} cells in vitro, but the division-specific frequencies of CD138^{+} cells
290 showed only modest decreases in *Dhrs7b*$^{\Delta/\Delta}$ B cells (Supplemental Fig. 4E). Thus, the reduction
291 of CD138^{+} cell differentiation appears to be due mostly to its dependence on survival to a
292 sufficient division count.
293

294 *Dhrs7b* inactivation was initiated prior to immunization in the preceding experiments.
295 Therefore, the impact of PexRAP deficiency on GC and the Ab response in such a setting might
296 be due exclusively to impairment of B cells, e.g., their reduced population expansion, prior to
297 their entry into GC. Alternatively, the effects could also in part involve a requirement for
298 PexRAP-dependent metabolites within GC B cells. To test if *Dhrs7b* functions within GC, we
299 used conditional deletion of *Dhrs7b* driven by the *S1pr2-CreER*^{T2} transgene whose expression at
300 high levels marks GC B cells (69). Of note, experiments with a fate-marking reporter allele
301 showed that activated B cells that lack the GC B phenotype were not marked by this conditional
302 Cre after immunization with the NP-carrier approach (69). *Dhrs7b*$^{f/f}$; *S1pr2-CreER*^{T2} and control
303 *S1pr2-CreER*^{T2} (control) mice were immunized with SRBC, and tamoxifen was injected at a time
304 point after the initiation of GC to assure more fully that the inactivation of *Dhrs7b* would be in
305 GC B cells rather than pre-GC blasts (Figure 7A). Frequencies of GC B cells were substantially
306 lower in tamoxifen-treated *Dhrs7b*$^{f/f}$; *S1pr2*-CreER^{T2} mice (Figure 7B, C), whereas the overall
307 populations of CD138^{+} cells, and CD19^{+} B220^{+} plasmablasts (PBs) among them - almost all of
308 which would have developed prior to the induced loss-of-function - were normal (Figure 7D, E).
309 These data provide evidence that *Dhrs7b* expression within GC B cells influences them during
310 an Ab response. Collectively, these data indicate that an optimal GC response requires PexRAP
311 function in B cells, and the B cell-intrinsic functions of *Dhrs7b* promote the quantity and affinity
312 maturation of Ab responses, in part via net proliferation of B cells.
313
314 ***Dhrs7b* contributes to modulation of ROS and their impact on B cell population growth.**
315 Increased susceptibility to cell death after activation would be a mechanism that could
316 cause the reduced population expansion, GC, and Ab production. Consistent with earlier analyses
317 of LPS-stimulated B cells (70), we had noted that ROS levels were higher in GC B cells,
318 memory B cells (MBCs) and ASCs than in the naive B2 B cell pool (36). ROS can be produced
319 in activated B cells via diverse sources that include mitochondrial electron transport chain
320 function, NADPH oxidase activated by BCR engagement, and fatty acid oxidation in

321 peroxisomes (71-73). ROS can positively mediate signal transduction, but their steady-state
322 concentrations need to be calibrated because overproduction can have deleterious effect on cells,
323 for instance via lipid peroxidation at excessive rates (74-76). Endogenous antioxidant properties
324 have been imputed to plasmalogens because the vinyl ether bond is susceptible to reaction with
325 reactive oxygen, thereby scavenging ROS (48, 57-59). When we tested if *Dhrs7b* function is
326 critical for redox control in B cells, mitogen-stimulated *Dhrs7b*$^{\Delta/\Delta}$ B cells exhibited ~3 fold
327 higher signal and about a doubling when stained with fluorescent sensors of cellular and
328 mitochondrial ROS, respectively, compared to WT B cells *in vitro* (Fig. 8A-D). Iron- and copper-
329 dependent lipid peroxidation is considered to be a biological mechanism for ROS-mediated cell
330 death (75, 76). Lipid peroxidation measured by a fluorescent indicator (C11-Bodipy) in vitro was
331 enhanced in mitogen-activated *Dhrs7b*$^{\Delta/\Delta}$ B cells compared with WT controls (Fig. 8E). One
332 independent means of driving increased ROS and lipid peroxidation in B cells (supplemental Fig.
333 S5A) rapidly led to reduced cell viability and B cell numbers (Fig. 8F). Furthermore, in vitro
334 analyses indicated that B cells lacking PexRAP also exhibited increases in the activated
335 executioner caspase, cleaved caspase-3 (CC3) along with early apoptotic cells that are annexin
336 V^+ but exclude 7-aminoactinomycin D (Fig. 8G, H). These data indicate that *Dhrs7b* function
337 supports not only protection against cell death, but also control of cellular and mitochondrial
338 ROS levels and their impact on lipid modification. Of note, while H_2O_2 did not increase this
339 early apoptotic population (Supplemental Fig. SC), increasing ROS with menadione drove B cell
340 death preceded by annexin V^+ state without an increase in C11-Bodipy signal (Supplemental Fig.
341 S5D-G). We infer that rather than a single mode of death, increased ROS resulting from PexRAP
342 depletion stimulates at least two distinct modes of B cell death.
343
344 Consistent with the increased steady-state ROS and death, activated *Dhrs7b*$^{\Delta/\Delta}$ B cells
345 exhibited a defect in B cell population growth *in vivo* and *in vitro* (Fig. 2; Fig. 8A-H). The well-
346 established ROS scavenger, N-acetyl-L-cysteine (NAC), exerted a concentration-dependent
347 effect that improved the survival and population growth of PexRAP-deficient B cells (Fig. 8I).

348 We exploited the sub-maximal rescue by a lower concentration of NAC (1 mM) to explore if
349 peroxisomal oxidative metabolism might contribute to the toxicity observed when B cells are
350 PexRAP-depleted. Although thioridazine on its own provided no increase in the B cell
351 population growth, its combination with 1 mM NAC treatment improved growth of the
352 *Dhrs7b*$^{\Delta/\Delta}$ B cell population compared to either agent on its own (Fig. 8J). These data indicate
353 that sufficient generation of PexRAP-dependent products is crucial for B cell survival. Moreover,
354 this enzyme contributes - directly or indirectly - to a resolution or detoxification of ROS that is
355 critical for population growth of activated B cells.
356
357 ***Dhrs7b* in B cells affects their oxidative metabolism and ER mass.**
358 Our finding that mitochondrial ROS were increased prompted us to investigate how PexRAP
359 affects physiological functions by measuring respiration in activated B cells. Mitochondrial
360 stress tests with in vitro activated B lymphoblasts measured small but definite decreases in both
361 basal and maximal respiration (oxygen consumption rates, or OCR) (Fig. 9A-C). The altered
362 performance of mitochondria was associated with reductions in calculated ATP generation and
363 proton leak as well as a small decrease in spare respiratory capacity (SRC) (Fig. 9D-F,
364 respectively). In contrast, the rates of glucose-stimulated extracellular acidification - cytosolic
365 reactions and a surrogate that can approximate glycolytic activity - were unaffected (Fig. 9G).
366 Thus, the altered respiration did not reflect a decrease in all cell metabolism. Inasmuch as
367 peroxisomes and mitochondria form contacts and functionally interact with the ER, we measured
368 relative ER mass and found that the signal of the fluorophore ERTracker was consistently
369 reduced in PexRAP-depleted B cells (Fig. 9H, I). We infer that both mitochondrial function and
370 ER mass in B cells are promoted by their expression of PexRAP.
371

372 **DISCUSSION**

373 We have shown herein that B lymphocyte expression of an enzyme essential for biosynthesis
374 of a subset of ether phospholipids is crucial for part of the increases in their levels localized to
375 GC. Moreover, the genetic approach used to deplete B cells of PexRAP allowed us to show that
376 the B cell type-restricted gene, *Dhrs7b*, promotes B cell survival, proliferation, and GC size
377 along with affinity maturation and serum concentrations of Ag-specific Ab after immunization.
378 Taken together, this work establishes the predictive value of the discovery approach that
379 identified an unexpected feature of cellular biochemistry in GC and indicates that B cell-
380 autonomous generation of ether lipid species is crucial for B cell survival and the qualities of the
381 Ab elicited by immunization.

382

383 Using imaging mass spectrometry for discovery-based hypothesis generation, we had
384 reported that the concentrations of at least a dozen ether phospholipids are increased in splenic
385 GC relative to the remainder of the tissue (45). The analyses presented here confirm and extend
386 the observations, and provide evidence that after immunization, these concentrations increase
387 even in the primary B cell follicle, albeit to a modest degree when compared to the magnitude of
388 increases in GC, and in B cells activated ex vivo. The cell type-specific gene inactivation after
389 establishment of a pre-immune population establishes that an enzyme crucial for generation of a
390 number of plasmalogens has substantial effects on B lymphocyte physiology and function.
391 Plasmalogens and other ether lipids and phospholipids have long been shown to be major
392 constituents of lipid bilayers and cell membranes (48, 49, 57). However, remarkably little is
393 known about whether or not cell-intrinsic synthesis of ether lipids or the balance among their
394 specific molecular species matters for hematopoietic cells or in immunity. Several inborn errors
395 of metabolism in humans are attributable to loss-of-function mutations of genes encoding
396 peroxisomal proteins that impact ether lipid (and hence plasmalogen) synthesis (58) but affect
397 other critical processes as well [reviewed in (48, 58-62)]. Several of these - such as Zellweger

398 Syndrome and rhizomelic chondrodysplasia punctata (RCDP) - and the mouse models generated
399 to study mechanisms in these human disease, lead to severe neurological defects and early post-
400 partum death (57, 58). Whether or not lymphocyte development, homeostasis or function were
401 affected in these studies is not clear. Deficient generation of ether lipids is among many
402 abnormalities caused by elimination of fatty acid synthase (FAS) (46, 47). Acute inactivation of
403 *Fasn*, the gene encoding this enzyme, in young mature mice caused a decrease in spleen size
404 disproportionate to the reduction in neutrophils, which was the most profound hematological
405 consequence (46). In addition, circulating lymphocytes were reduced despite normal steady-state
406 representation in the marrow. In-trans cell-extrinsic functions of ether lipids have been noted
407 previously - specifically, as ligands for the invariant natural killer T cell receptor (77) or for a G-
408 protein coupled receptor on natural killer cells (78). As such, the widespread loss of FAS
409 function and the potential for indirect and pleiotropic effects of this enzyme deficiency left
410 unresolved what cells actually depend on their own synthesis of ether lipids.
411
412 PexRAP, the enzyme encoded by the *Dhrs7b* gene, generates intermediates vital for the
413 synthesis of some - but not all - ether lipids in cells such as neutrophils (46). Analyses of
414 neutrophil numbers and survival provided evidence that this enzyme can be crucial for a normal
415 membrane composition. Moreover, PexRAP promoted viability of this very short-lived cell type
416 whose membranes have a high plasmalogen content (46). The bloodborne population of
417 lymphocytes was reduced in the *Rosa*26-CreER^{T2}, *Dhrs7b*$^{f/f}$ mice (46), but the specific types of
418 lymphoid cell were not reported and the circulating cell number does not necessarily correlate
419 with that in spleen or other organs. Of note, although subject to points articulated in (53), the
420 interpretation that the neutrophil phenotype is due to insufficiency of ether lipids or
421 plasmalogens has been questioned based on alternative gene disruption results (54). Several
422 models of unconditional gene inactivation or mutation that drastically reduced the phospholipid

423 end-products were noted to have normal neutrophils [summarized in (54), albeit at older ages (4 -
424 7 mo) than those used in (46). As noted, however, there may be age-related changes in the
425 processes analyzed herein using young (age ~ 2 mo) mice (53). Moreover, cellular and
426 organismal selection for adaptation variants makes the results of acute loss-of-function inherently
427 different from unconditional loss and heterozygote parentage (53). The potential for toxicity
428 induced by 4OHT activation of CreER^{T2} was among concerns mooted about the earlier study of
429 neutrophils (54). This concern may have been extrapolated from papers that noted impairment in
430 earlier hematopoiesis when *Rosa26*-CreER^{T2} was combined with intensive regimens of
431 tamoxifen administration to infant mice (65, 79). Of note, such studies used individual doses
432 over 4-fold higher that those used herein, and delivered by gavage five times on a daily basis, yet
433 the IgM^{+} B cell population sizes in spleen and marrow were normal even in the face of reduced
434 erythropoiesis and thymopoiesis (65). Moreover, the analyses herein compared B lineage-
435 specific deletion to CreER$^{T2+/-}$, *Dhrs7b*$^{+/+}$ mice identically dosed in parallel with the test
436 subjects. Thus, the work herein indicates that PexRAP is essential for normal physiology and
437 function of mature B lymphocytes, in particular after their activation.
438
439 The findings are most consistent with a capacity for PexRAP function to contribute towards
440 B lymphocyte survival and effective proliferation by restraining both executioner caspase
441 activation and lipid peroxidation due to excessive ROS levels. These findings are consistent with
442 those obtained with neutrophils (46). On the surface such results might appear to present a
443 conundrum relative to work indicating that both fatty acyl-CoA reductase 1 and the enzyme that
444 later generates an alkenyl bond at a terminal step in plasmalogen biosynthesis are crucial for the
445 susceptibility of HT-1080 and 786-O tumor cell lines to ferroptosis (55). However, our data are
446 consistent with published evidence that PexRAP is needed for a narrower subset of ether lipids
447 than the broad requirement for FAS or fatty acyl-CoA reductases (46-49, 80, 81). Moreover,

448 molecular dissection of mechanisms in various non-hematopoietic cell types (including the
449 cancer line 786-O) showed that ether lipid biosynthesis can either promote susceptibility or
450 resistance to ferroptosis (82). Collectively, our findings suggest that for B cells the inactivation
451 of PexRAP tilts the balance toward death and reduced Ab - perhaps involving lower fractions of
452 poly-unsaturated fatty acids (PUFA) (82), or a lower ratio of plasmalogens (alkenyl linkages)
453 relative to alkyl-linked ether lipids.
454
455 PexRAP localizes to peroxisomes (35-37), and prior work has suggested both that
456 peroxisomes are increased in GC B cells and likely contribute to FAO by these cells (26). In line
457 with the possibility that this organelle may affect PexRAP-dependent survival, our data indicated
458 that specific inhibition of peroxisomal FAO could collaborate with sub-optimal ROS scavenging
459 to mitigate the reduced growth of activated B cells. However, recent findings show that PexRAP
460 also is expressed in the ER and is capable of contributing to ether lipid biosynthesis via catalysis
461 in this organelle in addition to or instead of the peroxisome (56). Thus, although ROS generated
462 in peroxisomes likely contribute to the stress experienced by PexRAP-deficient B cells, the
463 phenotypes observed herein may not reflect the need for the peroxisomal fraction of the enzyme.
464
465 Our findings with an intermediary in ether lipid biosynthesis add to an increasing body of
466 evidence that metabolism in B lymphocytes affects their differentiation or function (28-36).
467 Many sources and forms of Ab can be protective, while in several autoimmune diseases these
468 molecules can drive pathology (1, 2). The capacity to generate increased affinities and circulating
469 concentrations of Ab is an important factor both in protective immunity and auto-immune
470 disease. Antigen-independent, TLR-driven PC differentiation requires increased oxidative
471 phosphorylation (70), while oxidative metabolism in GC B cells promotes affinity maturation by
472 unknown mechanisms (33-35). While not the exclusive determinant of such properties, GC are

473 major sources of higher affinity Ab with a broader spectrum of specificities (9, 13, 14). GC
474 formation, size, and function depend on the efficiency of population growth for B cells in a phase
475 before they enter and take on characteristics of GC B cells, and then homeostatic and
476 differentiative processes while in the secondary follicle. Thus, while the findings with the post-
477 immunization inactivation of *Dhrs7b* using *S1pr2*-CreER^{T2} provide evidence that the expression
478 of PexRAP is important within GC B cells, the decreases of GC and affinity-matured Ab are
479 likely also to involve a pre-GC phase of clonal expansion. In any case, the rapidity of the effects
480 suggests that pharmacological inhibition of PexRAP may be a target in inflammatory disease in
481 which B cells participate, particularly in light of the potential for impacts on pro-inflammatory
482 neutrophils.
483
484
485
486
487

488 **MATERIALS & METHODS**

489

490 ***Reagents*** Monoclonal antibodies (mAb) against mouse CD40, CD90.2, B220 (CD45R), and
491 other mAbs (purified, biotinylated, or fluorophore-conjugated) were from BD Biosciences or
492 Tonbo Biosciences (San Diego CA) unless otherwise indicated. BAFF was from AdipoGen (San
493 Diego, CA). Recombinant mouse IL-4 and recombinant mouse IL-5 were from Peprotech
494 (Rocky Hill NJ). Glucose, 2-deoxyglucose, oligomycin, rotenone, antimycin A, carbonyl cyanide
495 4-phenylhydrazone (FCCP), N-acetyl-cysteine (NAC), thioridazine hydrochloride, H_2O_2, and 4-
496 hydroxytamoxifen (4-OHT) were from Sigma-Aldrich Chemicals (St. Louis MO), and
497 menadione from Cayman Chemicals (Ann Arbor, MI). Tamoxifen (Tmx) was from APExBio
498 Technology (Houston TX). NP-BSA and NP-PSA (for capture in ELISA) as well as NP-OVA
499 (for immunization) were obtained from Biosearch Technology (Novato CA). SRBCs (sheep red
500 blood cells) were from Thermo Fisher Scientific (Waltham MA). CellTrace™ Violet cell
501 proliferation kit, CM-H_2DCFDA, MitoSOX™ Red, and BODIPY™ 581/591 C11 were obtained
502 from Invitrogen (Waltham, MA).

503

504 ***Mice, immunizations, ELISA and ELISpot*** All animal protocols were reviewed and approved
505 by the Vanderbilt University Institutional Animal Care and Use Committee. Mice were housed in
506 ventilated micro-isolators under Specified Pathogen-Free conditions in a Vanderbilt University
507 Medical Center mouse facility and used both male and female mice at 6–8 weeks of age. For cell
508 type specific inactivation of *Dhrs7b* genes, *Dhrs7b*$^{f/f}$ mice (46) were crossed with *Rosa26*-
509 CreER^{T2} (46), *huCD20*-CerER^{T2} (30), or *S1pr2*-CreER^{T2} strains (51, 52), all on C57/BL6 genetic
510 background. Tamoxifen was administered as previously reported (25, 30). To control for
511 potential Cre toxicity, CreER^{T2} mice were similarly injected to use as wild-type (WT) controls.
512 Mice (ages ~ 8wk) were immunized with SRBCs (2×10^8 cells per mouse) and analyzed 1 week
513 after immunization as described (25, 45). Alternatively, mice were immunized and boosted by
514 i.p. injections [each of 100 μg NP_{16}-OVA (Biosearch Technologies, Novato, CA) emulsified in

515 100 μL of Imject™ Alum (Thermo Fisher Scientific, Pittsburgh, PA)] as described previously
516 (25, 30), and harvested for analyses 1 wk after the 2nd injection. Isotype-specific relative levels of
517 Ag-specific Ab were quantitated by capture ELISA using Ag (NP_{20}-BSA or NP_2-PSA for all- or
518 high-affinity hapten-specific Abs, respectively) followed by SBA Clonotyping System (Southern
519 Biotech, Birmingham AL), as described previously (25, 30). As previously described (30),
520 frequencies of Ab-secreting cells (ASCs) were analyzed by ELISpot and quantitated using an
521 ImmunoSpot Analyzer (Cellular Technology, Shaker Heights OH).
522
523 ***Cell cultures, proliferation assay, and reversion of population growth*** Splenic B
524 cells were purified (90-95%) using negative selection as previously described (30) or by positive
525 selection with anti-mouse B220 microbeads (Miltenyi Biotech, Auburn, CA). B cells (5×10^5
526 cells in 1 ml) were activated with anti-CD40 (1 μg/mL) and cultured with BAFF (10 ng/mL),
527 IL-4 (10 ng/mL), IL-5 (10 ng/mL) and 4-OHT (50 nM) in Iscoves Modified Dulbecco's Medium
528 (IMDM) supplemented with 10% Fetal Bovine Serum (FBS), 100 U/mL penicillin 100 μg/mL
529 streptomycin (Invitrogen), 3 mM L-glutamine, nonessential amino acids (Invitrogen), 0.1 mM 2-
530 ME (Sigma-Aldrich). To analyze the effect of ROS scavenger and inhibition of peroxisomal lipid
531 oxidation on population growth, bead-purified B cells from tamoxifen-treated *huCD20*-CerER^{T2}
532 or *Dhrs7b*$^{f/f}$; *huCD20*-CerER^{T2} mice were activated with anti-CD40, cultured with BAFF, IL-4
533 and IL-5 in the presence or absence of NAC (1 mM and 5 mM) and/or thioridazine·HCl (100
534 μM) for 5 days. For enhancement of ROS in WT B cells, purified B cells were analyzed 3 d after
535 activation as for ROS scavenging, but vehicle, H_2O_2 (200 μM) or menadione (8 μM) was added
536 at three different time points (overnight, 3 hours, and 1 hour prior to processing for flow
537 cytometry to counting and measurements of DCFDA, annexin V, and C11 Bodipy signals.
538 For the analysis of proliferation in vitro, B cells were purified by depleting CD90.2$^+$ T
539 cells and CD138$^+$ cells using biotinylated anti-CD90.2 Ab and biotinylated anti-CD138 Ab
540 followed by streptavidin-conjugated microbeads (iMag™; BD Bioscience), labeled with 5 μM
541 CellTrace™ Violet (CTV, Invitrogen), activated and cultured as above. To analyze proliferation

542 in vivo, B cells were purified, labeled with CTV, and injected intravenously into B cell deficient
543 μMT recipient mice. Mice were harvested at 4 days after adoptive transfer.
544
545 ***Flow cytometry - general and measurements of ROS, lipids peroxidation, and ER*** GC B
546 cells were identified as $GL7^+$ $CD95^+$ events in the viable $B220^+$ $dump^-$ gate (dump channel
547 consisting of one fluorophore for CD11b, CD11c, F4/80, Gr1, TCRβ, and 7AAD) , while
548 plasmablasts were defined as $B220^+$ $CD138^+$ $TACI^+$ $dump^-$ cells. For flow analyses of total
549 intracellular ROS and mitochondrial superoxide, B cells (1×10^6 cells) were washed with PBS
550 and stained with 1.25 μM CM-H_2DCFDA or 5 μM MitoSOX™ Red in PBS (20 min at 37°C),
551 respectively, then washed with 1% BSA containing PBS, and further stained with anti-B220,
552 anti-CD19, anti-CD138, and Ghost-BV510. To measure the lipid peroxidation, cultured B cells
553 (1×10^6) were washed with PBS and stained with 1.25 μM C11-BODIPY™ in PBS (20 min at
554 37°C), and washed with 1% BSA containing PBS followed by surface staining as above. To
555 analyze the level of endoplasmic reticulum (ER), B cells (1×10^6) were stained with 0.5 μM ER-
556 Tracker™ Green (Molecular Probes, Eugene OR) in Hank's Balanced Salt Solution with calcium
557 and magnesium (HBSS/Ca/Mg; Gibco) for 30 min at 37°C.
558
559 For measurements of cell death (78), cultured B cells ($1 \text{ x } 10^6$) were washed twice with PBS,
560 once with Annexin V binding buffer (10 mM HEPES, pH 7.4, 140 mM NaCl, 2.5 mM $CaCl_2$),
561 and then incubated (15 min at 20 C in the dark) with Annexin V-rPE, 7AAD, APC-conjugated
562 CD138, APC-Cy7-conjugated B220, e450-CD19. Cells were then washed with Annexin V
563 binding buffer and analyzed on the flow cytometer. To measure levels of cleaved caspase-3 (25),
564 an activated apoptosis executor, the cultured cells were rinsed with PBS after harvest, stained (15
565 min at 4 C) with 7AAD, APC-conjugated CD138, APC-Cy7-conjugated B220, e450-CD19,
566 washed (FBS, 1% v/v in PBS), then fixed with paraformaldehyde (4% w/v, 10 min at 20 C),
567 permeabilized with permeabilization buffer (saponin, 0.2% w/v with FBS 1% in PBS), stained
568 with FITC-conjugated Ab specific for cleaved caspase-3 (BD Biosciences), rinsed, and analyzed

569 by flow cytometry.

570

571 ***Immunohistochemistry, MALDI-IMS, and IMS data analysis*** Mice were immunized with
572 SRBC and spleens were harvested at 1 week after immunization. Spleens were snap frozen on
573 dry ice, and mounted to a cryostat chuck with a minimal amount of OCT (Thermo Fisher
574 Scientific, San Jose, CA). Frozen spleens were cut at 12 µm thickness using a Leica CM3050S
575 (Leica, IL, USA) at -20 ºC, fixed with 1% paraformaldehyde for 10 min, washed twice with PBS,
576 and blocked with M.O.M™ (Vector Lab) followed by incubation with GL7-FITC, anti-IgD-PE,
577 and anti-CD35-biotin Ab followed by streptavidin-conjugated Alex647at 4 °C. After the tile
578 scanning of spleen sections, GC size and numbers were quantified with FIJI Image J software.

579

580 For Matrix-Assisted Laser Desorption/Ionization (MALDI) Imaging Mass Spectrometry
581 (IMS), frozen spleens were cut as above, and mounting onto indium tin oxide (ITO) coated
582 microscope slides (Delta Technologies ETC). Slides were then vacuum desiccated for at least 30
583 minutes before matrix application. Pre-IMS autofluorescence (AF) images were acquired prior to
584 matrix application on a Zeiss Axio Scan Z1 Slide Scanner using the brightfield channel and the
585 DAPI (ex. 340-380 nm; em. 435-485 nm, blue), EGFP (ex. 450-490 nm; em. 500-550 nm,
586 green), DsRed (ex. 538-562 nm; em. 570-640 nm, red) filter cubes. After taking AF images, a
587 custom in-house developed sublimation device was used to apply the matrices 2,5-
588 dihydroxyacetophenone (DHA) and 1,5-diaminonaphthalene (DAN) (Sigma Aldrich, St. Louis,
589 MO, USA) to tissue sections for positive and negative ion mode analyses, respectively (78). For
590 immunized AID-GFP mice, the fluorescence emissions identified GC localization within the
591 section used next for IMS. Alternatively, two serial sections of immunized mice spleens were
592 used, one for 2D-IMS and the contiguous section for immunohistochemistry (IHC). Fluorescence
593 data were registered with the 2D-IMS visualizations of phospholipids to align images (45),
594 allowing quantitation of the ion intensities in specific m/z peaks within defined micro-anatomic
595 portions of the spleen (Fig. 4B). MALDI IMS data were acquired with a 10 µm pixel size (laser

596 spot size 8 µm) in full scan mode using a Bruker trapped ion mobility time-of-flight (timsTOF)
597 Flex mass spectrometer (Bruker Daltonics Billerica, MA, USA). Data were acquired with 250
598 shots per pixel and a mass range of *m/z* 200-2000. SCiLS (software Bruker Daltonics) was used
599 to process the data, normalize ion intensity, visualize ion images, and merge the images.
600
601 ***LC-MS for lipidomics*** To prepare samples, a one-phase method was used to extract lipids
602 (85). Briefly, 0.5 mL of MeOH/MTBE/$CHCl_3$ mix (1.3:1:1) was added to a frozen pellet of B-
603 cells (1x10^6 cells total), spiked with 10 uL EquiSPLASH-lipidomics internal standard mix
604 (Avanti Research), briefly vortexed and shaken gently for 20 min, followed by centrifugation at
605 20,000 x *g* for 15 min at 10°C. The supernatant was transferred to a clean Eppendorf tube,
606 evaporated under a gentle stream of N_2 gas, and resuspended in 100 uL methanol/$CHCl_3$ (9:1)
607 and 2uL were used for LC-HRMS (high-resolution MS) analysis. Each sample was injected two
608 times - one injection in positive ESI mode followed by one in negative mode. Pooled QCs were
609 injected to assess the performance of the LC and MS instruments at the beginning, in the middle
610 and at the end of each sequence. Discovery lipidomics data were acquired using a Vanquish
611 UHPLC (ultrahigh performance liquid chromatography) system interfaced to a Q Exactive HF
612 quadrupole/orbitrap mass spectrometer (Thermo Fisher Scientific).
613
614 Chromatographic separation was performed with a reverse-phase Acquity BEH C18 column
615 (1.7 mm, 2.1x150mm, Waters, Milford, MA) at a flow rate of 250 ul/min. Mobile phases were
616 made up of 10 mM ammonium formate and 0.1% formic acid in (A) H_2O/CH_3CN (40:60) and
617 in (B) CH_3CN/ iPrOH (10:90). Gradient conditions were as follows: 0–1 min, B = 20 %; 1–8
618 min, B = 20– 100 %; 8–10 min, B = 100 %; 10–10.5 min, B = 100–20 %; 10.5–15 min, B =
619 20%. The total chromatographic run time was 15 min. Mass spectra were acquired over a
620 precursor ion scan range of m/z 200 to 1,600 at a resolving power of 60,000 using the
621 following HESI-II source parameters: spray voltage 4 kV (3 kV in negative mode); capillary
622 temperature 250°C; S-lens RF level 60 V; N_2 sheath gas 40; N_2 auxiliary gas 10; auxiliary gas
623 temperature 350°C. MS/MS spectra were acquired for the top-seven most abundant precursor

624 ions with an MS/MS AGC target of 1e5, a maximum MS/MS injection time of 100 ms, and a
625 normalized collision energy of 15, 30, 40. High resolution mass spectrometry data were
626 processed with MS-DIAL version 4.70 in lipidomics mode (86). MS1, and MS2 tolerances
627 were set to 0.01 and 0.025 Da respectively. Minimum peak height was set to 30,000 to
628 decrease the number of false positive hits. Peaks were aligned on a quality control (QC)
629 reference file with RT tolerance of 0.1 min and mass tolerance of 0.015 Da. Default lipid
630 library was used (Msp20210527163602_converted.lbm2), solvent type was set to $HCOONH_4$
631 to match the solvent used for separation, and the identification score cut off was set to 80%.
632 All lipid classes were made available for the search. After lipid identification was completed,
633 MS-DIAL results were exported into Excel and cleaned using minimum RSD for QC samples
634 set to 20% and minimum ratio of QC to Blank set to 10. For species identified in both
635 PexRAP-depleted (*Dhrs7b* Δ/Δ) B cells and controls, mean levels (areas under peak curves)
636 and their variance were analyzed in Excel.
637

638 ***Metabolic flus analyses*** Oxygen Consumption Rate (OCR) were measured using Seahorse
639 XF96 extracellular flux analyzer (Agilent Technology, Santa Clara, CA) as described previously
640 (30). Briefly, in vitro activated B cells were washed twice, resuspended in XF Base Media
641 (Agilent Technologies) supplemented with 2 mM L-glutamine, and equal numbers of B cells (2
642 $\times 10^5$) were plated on extracellular flux assay plates (Agilent Technologies) coated with 2.5
643 µg/mL CellTak (Corning) according to the manufacturer's protocol. Before extracellular flux
644 analysis, B cells were rested (25 minutes at 37°C, atmospheric CO_2) in XF Base Media. OCR
645 and ECAR were measured before and after the sequential addition of 1.5 µM oligomycin, 0.5
646 µM FCCP and 0.5 µM rotenone/antimycin A.
647
648

649 **ACKNOWLEDGEMENTS**

650 The experimental work was funded by NIH Grants to VUMC [R01 AI113292 (M.R.B), R01
651 HL106812 (M.R.B.), followed by R21 AI164760 (M.R.B.) and departmental funds]. Mass
652 spectrometry imaging was supported in part by NIH grant P41 GM103391 to Vanderbilt

653 University (R.M.C.). Additional support for M. A. J. was provided by the National Science
654 Foundation, NSF DGE-1445197. NIH Shared Instrumentation Grant 1S10OD018015 as well
655 as scholarships via the Cancer Center Support Grant (CA068485) and Diabetes Research Center
656 (DK0205930) helped defray costs of Vanderbilt Cores. We thank J. Cyster for generously
657 expediting shipment of *S1pr2*-CreERT2 breeding stock, and Vanderbilt institutional cores (High-
658 Throughput Screening; Flow Cytometry Shared Resource; Mass Spectrometry Shared Resource;
659 Cell & Developmental Biology) for equipment, expertise, and assistance.
660
661
662
663 **References**

664 1. Geyer CE, Mes L, Newling M, den Dunnen J, Hoepel W. 2021. Physiological and
665 pathological inflammation induced by antibodies and pentraxins. *Cells* **10:** 1175.
666 2. McGettigan SE, Debes GF. 2021. Immunoregulation by antibody secreting cells
667 in inflammation, infection, and cancer. *Immunol Rev*. **303:** 103-118.
668 3. Lu LL, Suscovich TJ, Fortune SM, Alter G. 2018. Beyond binding: antibody effector
669 functions in infectious diseases. *Nat Rev Immunol.* **18:** 46-61.
670 4. Allman D, Pillai S. 2008. Peripheral B cell subsets. *Curr Opin Immunol.* **20**: 149-157.
671 5. Martin F, Kearney JF. 2000. B-cell subsets and the mature preimmune repertoire. Marginal
672 zone and B1 B cells as part of a "natural immune memory". *Immunol Rev.* **175:** 70-79.
673 6. MacLennan, IC, Toellner KM, Cunningham AF, Serre K, Sze DM, Zuniga E, Cook MC,
674 Vinuesa CG. 2003. Extrafollicular antibody responses. *Immunol Rev* **194:** 8-18.
675 7. Hsu, M. C., K. M. Toellner, C. G. Vinuesa, and I. C. Maclennan. 2006. B cell clones that
676 sustain long-term plasmablast growth in T-independent extrafollicular antibody
677 responses. *Proc Natl Acad Sci USA* **103:** 5905-5510.
678 8. Rajewsky K. 1996. Clonal selection and learning in the antibody system. *Nature* **81:** 751-
679 758.

680 9. Boothby MR, Hodges E, Thomas JW. 2019. Molecular regulation of peripheral B cells and
681 their progeny in immunity. *Genes Dev.* **33:** 26-48.
682 10. Rubtsova K, Rubtsov AV, van Dyk LF, Kappler JW, Marrack P. 2013. T-box transcription
683 factor T-bet, a key player in a unique type of B-cell activation essential for effective viral
684 clearance. *Proc Natl Acad Sci USA* 110: E3216-24.
685 11. Alemán OR, Rosales C. 2023. Human neutrophil Fc gamma receptors: different buttons for
686 different responses. *J Leukoc Biol.* 114: 571-584.
687 12. Xu Z, Zan H, Pone EJ, Mai T, Casali P. 2012.Immunoglobulin class-switch recombination:
688 induction, targeting, and beyond. *Nat Rev Immunol.* **12:** 517-531.
689 13. Elsner RA, Shlomchik MJ. 2020. Germinal Center and extrafollicular B cell responses in
690 vaccination, immunity, and autoimmunity. *Immunity* **53:** 1136-1150.
691 14. Good-Jacobson, K. L., and M. J. Shlomchik. 2010. Plasticity and heterogeneity in the
692 generation of memory B cells and long-lived plasma cells: the influence of germinal
693 center interactions and dynamics. *J Immunol* **185:** 3117-3125.
694 15. Shlomchik M, Mascelli M, Shan H, Radic MZ, Pisetsky D, Marshak-Rothstein A, Weigert
695 M. 1990. Anti-DNA antibodies from autoimmune mice arise by clonal expansion and
696 somatic mutation. *J Exp Med*. **171:** 265-292.
697 16. Thomas JW, Hulbert C. 1996. Somatically mutated B cell pool provides precursors for
698 insulin antibodies. *J Immunol.* **157:** 763-771.
699 17. De Silva NS, Klein U. 2015. Dynamics of B cells in germinal centres. *Nat Rev Immunol.* **15:**
700 137-148.
701 18. Cyster JG, Allen CDC. 2019. B cell responses: Cell interaction dynamics and decisions. *Cell*
702 **177:** 524-540.
703 19. Victora, G. D., and M. C. Nussenzweig. 2022. Germinal Centers. *Annu Rev Immunol* **40:**
704 413-442.

705 20. Guttormsen HK, Sharpe AH, Chandraker AK, Brigtsen AK, Sayegh MH, Kasper DL. 1999.
706 Cognate stimulatory B-cell-T-cell interactions are critical for T-cell help recruited by
707 glyco-conjugate vaccines. *Infect Immun.* **67:** 6375-6384.
708 21. Kim W, Zhou JQ, Horvath SC, Schmitz AJ, Sturtz AJ, Lei T, Liu Z, Kalaidina E, Thapa M,
709 Alsoussi WB, Haile A, Klebert MK, Suessen T, Parra-Rodriguez L, Mudd PA, Whelan
710 SPJ, Middleton WD, Teefey SA, Pusic I, O'Halloran JA, Presti RM, Turner JS, Ellebedy
711 AH. 2022. Germinal centre-driven maturation of B cell response to mRNA vaccination.
712 *Nature* **604:** 141-145.
713 22. Roco JA, Mesin L, Binder SC, Nefzger C, Gonzalez-Figueroa P, Canete PF, Ellyard J, Shen
714 Q, Robert PA, Cappello J, Vohra H, Zhang Y, Nowosad CR, Schiepers A, Corcoran LM,
715 Toellner KM, Polo JM, Meyer-Hermann M, Victora GD, Vinuesa CG. 2019. Class-
716 switch recombination occurs infrequently in Germinal Centers. *Immunity* **51:** 337-350.
717 23. Gitlin AD, Shulman Z, Nussenzweig MC 2014. Clonal selection in the germinal centre by
718 regulated proliferation and hypermutation. *Nature* **509:** 637-40.
719 24. Vinuesa CG, Linterman MA, Yu D, MacLennan IC. 2016. Follicular helper T cells. *Annu*
720 *Rev Immunol.* **34:** 335-368.
721 25. Mayer CT, Gazumyan A, Kara EE, Gitlin AD, Golijanin J, Viant C, Pai J, Oliveira TY,
722 Wang Q, Escolano A, Medina-Ramirez M, Sanders RW, Nussenzweig MC. 2017. The
723 micro-anatomic segregation of selection by apoptosis in the germinal center. *Science* **358:**
724 eaao2602.
725 26. Chapman NM, Chi H. 2022. Metabolic adaptation of lymphocytes in immunity and disease.
726 *Immunity* **55:** 14-30.
727 27. Bacigalupa ZA, Landis MD, Rathmell JC. 2024. Nutrient inputs and social metabolic control
728 of T cell fate. *Cell Metab.* **36:** 10-20.

729 28. Jellusova J. 2020. Metabolic control of B cell immune responses. *Curr Opin Immunol.* **63:**
730 21-28.
731 29. Boothby MR, Brookens SK, Raybuck AL, Cho SH. 2022. Supplying the trip to antibody
732 production-nutrients, signaling, and the programming of cellular metabolism in the
733 mature B lineage. *Cell Mol Immunol.* **19:** 352-369.
734 30. O'Neill LA, Kishton RJ, Rathmell J. 2016. A guide to immunometabolism for
735 immunologists. *Nat Rev Immunol*. **16:** 553-565.
736 31. Cho, S. H., A. L. Raybuck, K. Stengel, M. Wei, T. C. Beck, E. Volanaki, J. W. Thomas, S.
737 Hiebert, V. H. Haase, and M. R. Boothby. 2016. Germinal centre hypoxia and regulation
738 of antibody qualities by a hypoxia response system. *Nature* **537:** 234-237.
739 32. Weisel, F. J., S. J. Mullett, R. A. Elsner, A. V. Menk, N. Trivedi, W. Luo, D. Wikenheiser,
740 W. F. Hawse, M. Chikina, S. Smita, L. J. Conter, S. M. Joachim, S. G. Wendell, M. J.
741 Jurczak, T. H. Winkler, G. M. Delgoffe, and M. J. Shlomchik. 2020. Germinal center B
742 cells selectively oxidize fatty acids for energy while conducting minimal glycolysis. *Nat*
743 *Immunol* **21:** 331-342.
744 33. Chen D, Wang Y, Manakkat Vijay GK, Fu S, Nash CW, Xu D, He D, Salomonis N, Singh H,
745 Xu H. 2021. Coupled analysis of transcriptome and BCR mutations reveals role of
746 OXPHOS in affinity maturation. *Nat Immunol.* 22: 904-913.
747 34. Urbanczyk S, Baris OR, Hofmann J, Taudte RV, Guegen N, Golombek F, Castiglione K,
748 Meng X, Bozec A, Thomas J, Weckwerth L, Mougiakakos D, Schulz SR, Schuh W,
749 Schlotzer-Schrerhardt U, Steinmetz TD, Brodesser S, Wiesner RJ, Mielenz D. 2022.
750 Mitochondrial respiration in B lymphocytes is essential for humoral immunity by
751 controlling the flux of the TCA cycle. *Cell Rep.* **39:** 110912.
752 35. Yazicioglu Y. F., E. Marin, C. Sandhu, S. Galiani, I. G. A. Raza, M. Ali, B. Kronsteiner, E.
753 B. Compeer, M. Attar, S. J. Dunachie, M. L. Dustin, and A. J. Clarke. 2023. Dynamic

754 mitochondrial transcription and translation in B cells control germinal center entry and
755 lymphomagenesis. *Nat Immunol.* **24:** 991-1006.
756 36. Brookens SK, Cho SH, Paik Y, Meyer K, Raybuck AL, Park C, Greenwood DL, Rathmell
757 JC, Boothby MR. 2024. Plasma cell differentiation, antibody quality, and initial germinal
758 center B cell population depend on glucose influx rate. *J Immunol.* **212:** 43-56.
759 37. Olenchock BA, Rathmell JC, Vander Heiden MG. 2017. Biochemical underpinnings of
760 immune cell metabolic phenotypes. *Immunity* **46:** 703-713.
761 38. Kong H, Chandel NS. 2018. Regulation of redox balance in cancer and T cells. *J Biol Chem*.
762 **293:** 7499-7507.
763 39. Addabbo F, Montagnani M, Goligorsky MS. 2009. Mitochondria and reactive oxygen
764 species. *Hypertension* **53:** 885-892.
765 40. Zorov DB, Juhaszova M, Sollott SJ. 2014. Mitochondrial reactive oxygen species (ROS) and
766 ROS-induced ROS release. *Physiol Rev.* **94:** 909-950.
767 41. Jellusova, J., M. H. Cato, J. R. Apgar, P. Ramezani-Rad, C. R. Leung, C. Chen, A. D.
768 Richardson, E. M. Conner, R. J. Benschop, J. R. Woodgett, and R. C. Rickert. 2017.
769 Gsk3 is a metabolic checkpoint regulator in B cells. *Nat Immunol* **18:** 303-312.
770 42. Li L, Feng C, Qin J, Li D, Liu M, Han S, Zheng B. 2021. Regulation of humoral immune
771 response by HIF-1α-dependent metabolic reprogramming of the germinal center reaction.
772 *Cell Immunol.* **367:** 104409.
773 43. Nakagawa R, Llorian M, Varsani-Brown S, Chakravarty P, Camarillo JM, Barry D, George
774 R, Blackledge NP, Duddy G, Kelleher NL, Klose RJ, Turner M, Calado DP. 2023. Epi-
775 microRNA mediated metabolic reprogramming ensures affinity maturation. *bioRxiv*
776 [Preprint]. 2023 Oct 31:2023.07.31.551250.

777 44. Jain IH, Calvo SE, Markhard AL, Skinner OS, To TL, Ast T, Mootha VK. 2020. Genetic
778 screen for cell fitness in high or low oxygen highlights mitochondrial and lipid
779 metabolism. *Cell* **181:** 716-727.e11.
780 45. Jones MA, Cho SH, Patterson NH, Van de Plas R, Spraggins JM, Boothby MR, Caprioli
781 RM. 2020. Discovering new lipidomic features using cell type-specific fluorophore
782 expression to provide spatial and biological specificity in a multimodal workflow with
783 MALDI Imaging Mass Spectrometry. *Anal Chem.* **92:** 7079-7086.
784 46. Lodhi IJ, Wei X, Yin L, Feng C, Adak S, Abou-Ezzi G, Hsu FF, Link DC, Semenkovich CF.
785 2015. Peroxisomal lipid synthesis regulates inflammation by sustaining neutrophil
786 membrane phospholipid composition and viability. *Cell Metab.* **21:** 51-64.
787 47. Lodhi IJ, Yin L, Jensen-Urstad AP, Funai K, Coleman T, Baird JH, El Ramahi MK, Razani
788 B, Song H, Fu-Hsu F, Turk J, Semenkovich CF. 2012. Inhibiting adipose tissue
789 lipogenesis reprograms thermogenesis and PPARγ activation to decrease diet-induced
790 obesity. *Cell Metab.* **16:** 189-201.
791 48. Dean JM, Lodhi IJ. 2018. Structural and functional roles of ether lipids. *Protein Cell* **9:** 196-
792 206.
793 49. Honsho M, Fujiki Y. 2023. Regulation of plasmalogen biosynthesis in mammalian cells and
794 tissues. *Brain Res Bull.* **194:** 118-123.
795 50. Werner ER, Swinkels D, Juric V, Dorninger F, Baes M, Keller MA, Berger J, Watschinger
796 K. 2023. Normal plasmalogen levels are maintained in tissues from mice with
797 hepatocyte-specific deletion in peroxin 5. *Brain Res Bull.* **193:** 158-165.
798 51. Dorninger F, Werner ER, Berger J, Watschinger K. 2022. Regulation of plasmalogen
799 metabolism and traffic in mammals: The fog begins to lift. *Front Cell Dev Biol.* **10:**
800 946393.

801 52. Kuerschner L, Richter D, Hannibal-Bach HK, Gaebler A, Shevchenko A, Ejsing CS, Thiele
802 C. 2012. Exogenous ether lipids predominantly target mitochondria. *PLoS One* **7:**
803 e31342.
804 53. Lodhi IJ, Link DC, Semenkovich CF. 2015. Acute ether lipid deficiency affects neutrophil
805 biology in mice. *Cell Metab.* **21:** 652-653.
806 54. Dorninger F, Wiesinger C, Braverman NE, Forss-Petter S, Berger J. 2015. Ether lipid
807 deficiency does not cause neutropenia or leukopenia in mice and men. *Cell Metab.* **21:**
808 650-651.
809 55. Cui W, Liu D, Gu W, Chu B. 2021. Peroxisome-driven ether-linked phospholipids
810 biosynthesis is essential for ferroptosis. *Cell Death Differ.* **28:** 2536-2551.
811 56. Honsho M, Tanaka M, Zoeller RA, Fujiki Y. 2020. Distinct functions of acyl/alkyl
812 dihydroxyacetonephosphate reductase in peroxisomes and endoplasmic reticulum. *Front*
813 *Cell Dev Biol.* **8:** 855.
814 57. Braverman NE, Moser AB. 2012. Functions of plasmalogen lipids in health and disease.
815 *Biochim Biophys Acta* **1822:** 1442-1452.
816 58. Gorgas K, Teigler A, Komljenovic D, Just WW. 2006. The ether lipid-deficient mouse:
817 tracking down plasmalogen functions. *Biochim Biophys Acta* **1763:** 1511-1526.
818 59. Jiménez-Rojo N, Riezman H. 2019. On the road to unraveling the molecular functions of
819 ether lipids. *FEBS Lett.* **93:** 2378-2389.
820 60. Rangholia N, Leisner TM, Holly SP. 2021. Bioactive ether lipids: Primordial modulators of
821 cellular signaling. *Metabolites* **11:** 41.
822 61. Bozelli JC Jr, Azher S, Epand RM. 2021. Plasmalogens and chronic inflammatory diseases.
823 *Front Physiol.* **12:** 730829.
824 62. Wallner S, Schmitz G. 2011. Plasmalogens the neglected regulatory and scavenging lipid
825 species. *Chem Phys Lipids* **164:** 573-589.

826 63. Friedrich, G, Soriano, P. 1991. Promoter traps in embryonic stem cells: A genetic screen to
827 identify and mutate developmental genes in mice. *Genes Devel*. **5:** 1513–1523.
828 64. Shapiro-Shelef M, Lin KI, Savitsky D, Liao J, Calame K. 2005. Blimp-1 is required for
829 maintenance of long-lived plasma cells in the bone marrow. *J Exp Med.* **202:** 1471-1476.
830 65. Higashi AY, Ikawa T, Muramatsu M, Economides AN, Niwa A, Okuda T, Murphy AJ, Rojas
831 J, Heike T, Nakahata T, Kawamoto H, Kita T, Yanagita M. 2009. Direct hematological
832 toxicity and illegitimate chromosomal recombination caused by the systemic activation of
833 CreERT2. *J Immunol.* **182:** 5633-5640.
834 66. Uhmann A, Dittmann K, Wienands J, Hahn H. 2009. Comment on "Direct hematological
835 toxicity and illegitimate recombination caused by the systemic activation of CreERT2". *J*
836 *Immunol.* **183:**2891.
837 67. Khalil AM, Cambier JC, Shlomchik MJ. 2012. B cell receptor signal transduction in the GC
838 is short-circuited by high phosphatase activity. *Science* **336:** 1178-1181.
839 68. Inoue T, Kurosaki T. 2024. Memory B cells. *Nat Rev Immunol.* **24:** 5-17.
840 69. Shinnakasu R, Inoue T, Kometani K, Moriyama S, Adachi Y, Nakayama M,
841 Takahashi Y, Fukuyama H, Okada T, Kurosaki T. 2016. Regulated selection of germinal-
842 center cells into the memory B cell compartment. *Nat Immunol.* **17:** 861-869.
843 70. Price MJ, Patterson DG, Scharer CD, Boss JM. 2018. Progressive upregulation of oxidative
844 metabolism facilitates plasmablast differentiation to a T-independent antigen.
845 *Cell Rep.* **23:** 3152-3159.
846 71. Capasso M, Bhamrah MK, Henley T, Boyd RS, Langlais C, Cain K, Dinsdale D, Pulford K,
847 Khan M, Musset B, Cherny VV, Morgan D, Gascoyne RD, Vigorito E, DeCoursey TE,
848 MacLennan IC, Dyer MJ. 2010. MacLennan IC, Dyer MJ. 2010. HVCN1 modulates
849 BCR signal strength via regulation of BCR-dependent generation of reactive oxygen
850 species. *Nat Immunol*. **11:** 265-272.

851 72. Wheeler ML, Defranco AL. 2012. Prolonged production of reactive oxygen species in
852 response to B cell receptor stimulation promotes B cell activation and proliferation. *J*
853 *Immunol.* **189:** 4405-4416.
854 73. Tsubata T. 2020. Involvement of reactive oxygen species (ROS) in BCR signaling as a
855 second messenger. *Adv Exp Med Biol*. **1254:** 37-46.
856 74. Jiang X, Stockwell BR, Conrad M. 2021. Ferroptosis: mechanisms, biology and role in
857 disease. *Nat Rev Mol Cell Biol.* **22:** 266-282.
858 75. Nordgren M, Fransen M. 2014. Peroxisomal metabolism and oxidative stress. *Biochimie* **98:**
859 56-62.
860 76. Liang D, Minikes AM, Jiang X. 2022. Ferroptosis at the intersection of lipid metabolism and
861 cellular signaling. *Mol Cell* **82:** 2215-2227.
862 77. Facciotti F, Ramanjaneyulu GS, Lepore M, Sansano S, Cavallari M, Kistowska M, Forss-
863 Petter S, Ni G, Colone A, Singhal A, Berger J, Xia C, Mori L, De Libero G. 2012.
864 Peroxisome-derived lipids are self antigens that stimulate invariant natural killer T cells
865 in the thymus. *Nat Immunol.* 3: 474-480.
866 78. Hossain MS, Mawatari S, Fujino T. 2022. Plasmalogen-mediated activation of GPCR21
867 regulates cytolytic activity of NK cells against the target cells. *J Immunol.* **209:** 310-325.
868 79. Rossi M, Salomon A, Chaumontel N, Molet J, Bailly S, Tillet E, Bouvard C. 2023. Warning
869 regarding direct hematological toxicity of tamoxifen-activated CreERT2 in young
870 Rosa26-CreERT2 mice. *Sci Rep*. **13:** 5976.
871 80. Lodhi IJ, Semenkovich CF. 2014. Peroxisomes: a nexus for lipid metabolism and cellular
872 signaling. *Cell Metab.* **19:** 380-392.
873 81. He A, Dean JM, Lodhi IJ. 2021. Peroxisomes as cellular adaptors to metabolic and
874 environmental stress. *Trends Cell Biol*. **31:** 656-670.

875 82. Zou Y, Henry WS, Ricq EL, Graham ET, Phadnis VV, Maretich P, Paradkar S, Boehnke N,
876 Deik AA, Reinhardt F, Eaton JK, Ferguson B, Wang W, Fairman J, Keys HR, Dančík V,
877 Clish CB, Clemons PA, Hammond PT, Boyer LA, Weinberg RA, Schreiber SL. 2020.
878 Plasticity of ether lipids promotes ferroptosis susceptibility and evasion. *Nature* **585:**
879 603-608.
880 83. Esselman AB, Patterson NH, Migas LG, Dufresne M, Djambazova KV, Colley ME, Van de
881 Plas R, Spraggins JM. 2023. Microscopy-Directed Imaging Mass Spectrometry for Rapid
882 High Spatial Resolution Molecular Imaging of Glomeruli. *J Am Soc Mass Spectrom.* **34:**
883 1305-1314.
884 84. Lee K, Heffington L, Jellusova J, Nam KT, Raybuck A, Cho SH, Thomas JW, Rickert
885 RC, Boothby M. 2013. Requirement for Rictor in homeostasis and function of mature B
886 lymphoid cells. *Blood* **122:** 2369-2379.
887 85. Pellegrino RM, Di Veroli A, Valeri A, Goracci L, Cruciani G. 2014. LC/MS lipid profiling
888 from human serum: a new method for global lipid extraction. *Anal Bioanal Chem*. **406:**
889 7937-7948.
890 86. Tsugawa H, Ikeda K, Takahashi M, Satoh A, Mori Y, Uchino H, Okahashi N, Yamada Y,
891 Tada I, Bonini P, Higashi Y, Okazaki Y, Zhou Z, Zhu Z-J, Koelmel J, Cajka T, Fiehn O,
892 Saito K, Arita M, Arita M. 2020. A lipidome atlas in MS-DIAL 4. *Nat Biotechnol*. **38:**
893 1159-1163.
894 87. Tao L, Lemoff A, Wang G, Zarek C, Lowe A, Yan N, Reese TA. 2020. Reactive oxygen
895 species oxidize STING and suppress interferon production. *Elife* **9:** e57837. doi:
896 10.7554/eLife.57837.
897

898 **Figure Legends**

899

900 **Figure 1. PexRAP promotes GC response.** (A) Schematic of immunization with SRBC after
901 inactivation of *Dhrs7b* in adult mice. Mice (*Rosa26*-CreER^{T2}; *Dhrs7b*$^{+/+}$*, or Rosa26*-CreER^{T2};
902 *Dhrs7b*^{ff}) were treated with tamoxifen, immunized with SRBC*,* and harvested 1 wk after
903 immunization, as described in *Materials and Methods*. (B) Deletion efficiency of *Dhrs7b*
904 conditional alleles. B and T lymphocytes were isolated from spleens of *Rosa26*-CreER^{T2} or
905 *Dhrs7b*$^{f/f}$*;Rosa26*-CreER^{T2} mice after in vivo tamoxifen injections followed by immunization
906 with SRBC. WT and *Dhrs7b*$^{\Delta/\Delta}$ were analyzed by immunoblotting with antibodies directed
907 against PexRAP (protein product of *Dhrs7b*) and actin (internal loading control). (C, D) PexRAP
908 acutely regulates B cell numbers. Representative flow plots of viable splenic B cells (C) and
909 aggregate data for three biologically independent replicate experiments (D) (n = 8 WT and 7
910 cKO). For data on T cells, see supplemental data Fig. S1A-C. (E, F) Effect of PexRAP on GC B
911 cell response. Flow plots of GL7^{+} CD95^{+} GC B cells among viable B cells (E), and aggregated
912 frequencies and numbers of GC B cells, as indicated, in the three replicate experiments (F). (G,
913 H) PexRAP impact on GC response. After tamoxifen injections, *Dhrs7b* deficient mice [*Rosa26*-
914 CreER^{T2}; *Dhrs7b*^{ff} (46)] and WT controls (*Rosa26*-CreER^{T2}) were immunized with SRBC and
915 analyzed 7 d later, as in Fig. 1A-F. Data on gating strategy, GC counts per unit area and LZ area
916 are in Supplemental data Fig. 1D-F. (G, H) Shown are representative images from
917 immunofluorescence staining of spleens with the indicated Ab in two independent experiments
918 (5 WT vs 4 *Dhrs7b* cKO), showing a low-power overview with many follicles (G) and a
919 representative higher-magnification image to better delineate primary and secondary follicles
920 (H). (I) Quantitation of number (left panel) and size (right panel) of GC in spleen sections, with
921 GL7-positive, IgD-negative areas that include both CD35+ (LZ) and CD35- (DZ) areas. Mann-
922 Whitney U test was used to calculate p values.

923

924 **Figure 2. PexRAP promotes proliferation of B cells.** (A) Schematic of *Dhrs7b* inactivation in
925 mature mice via tamoxifen treatment and a B cell type-specific conditional allele. Mice
926 (*huCD20*-CreER^{T2}; *Dhrs7b*$^{+/+}$*, or huCD20*-CreER^{T2}; *Dhrs7b*^{ff}) were injected with tamoxifen (d1,
927 3, 5) and harvested at day 10. (B) Deletion efficiency of conditional *Dhrs7b* alleles. After in vivo
928 tamoxifen injections, B cells were isolated from spleens of *hCD20*-CreER^{T2} or *Dhrs7b*$^{f/f}$*;*

929 *hCD20*-CreER^{T2} mice, as indicated, and analyzed by immunoblotting as in Fig. 1B. (C) PexRAP
930 and the maintenance of B cells. Shown are the frequencies and the numbers of CD19^{+} B220^{+} B
931 cells among viable lymphocytes in spleen (left and right panels, respectively). Data are pooled
932 from four independent replicate experiments (n = 12 WT and 12 cKO). Shown in feather plots
933 are the means, with whiskers that extend to the minimum and maximum values and boxes that
934 outline upper and lower quartile values with the midline identifying the median.(D-F) PexRAP
935 regulates B cell proliferation in vivo. CTV-labeled B cells were adoptively transferred into μMT
936 recipient mice and analyzed 4 days thereafter. Shown are the frequencies of B220^{+} CD19^{+} events
937 among splenocytes in the viable cell gate (D), along with representative flow plots of CTV
938 partitioning and surface IgD in B cell gates (E) and aggregated frequencies of divided B cells
939 from five independent replicate experiments (F) (n =10 WT and 11 cKO). Additional data on the
940 IgD^{neg} population are in supplemental Fig.1J. (G-I) PexRAP promotes B cell proliferation in
941 vitro. After in vivo tamoxifen injections, bead-purified B cells from spleens of CreER^{T2} mice
942 (WT and *Dhrs7b*$^{\Delta/\Delta}$*, i.e., cKO*) were stained with Cell Trace Violet (CTV), activated and
943 cultured 4 days in anti-CD40, BAFF, IL-4, IL-5 and 4-hydroxytamoxifen in three biologically
944 independent experiments totaling 6 WT and 7 cKO mice). (G) Representative flow-cytometric
945 analysis of CTV partitioning. (H) Quantified frequencies of divided >3 times. (I) Numbers of B
946 cells recovered at the end of the cultures.
947
948 **Figure 3. B cell expression of PexRAP is essential for normal concentrations of most ether**
949 **phospholipids.** Splenic B cells (CreER^{T2+} or CreER^{T2+}, *Dhrs7b* Δ/Δ) from tamoxifen-injected
950 mice were analyzed by LC-MS-MS either directly ex vivo ("Naive") or after activation and
951 culture (48 h) ("Activated") as in Fig. 2. Shown are z-scored heat maps for the relative
952 abundance of subsets of ether and plasmalogen phospholipids and lysophospholipids identified
953 by exact mass and secondary fragmentation in (A) positive and/or (B) negative ion modes. More
954 species are displayed in Supplemental Fig. 2. (C) Quantitated peak areas for activation-induced
955 increases ('fold-induction' ratios of activated/resting, plotted on $\log_{10}$ scale) for the indicated
956 ether, plasmalogen, and diacyl (non-ether) phospholipids in the PexRAP-sufficient and -depleted
957 B cells. * denotes species for which P<0.05 for the effect of *Dhrs7b* inactivation. (D) Shown are
958 the raw values of mean peak areas for the indicated species in the freshly purified and the
959 activated B cells of the indicated genotypes, as indicated. (Three independent samples from

960 individual mice of each genotype were analyzed.) * $p<0.05$, ** $p<0.01$ by unpaired Student's. t-
961 test. Additional data including controls comparing B cells of unmanipulated B6 mice to those
962 expressing CreER^{T2} and injected with tamoxifen are in Supplemental Fig. 2.
963
964 **Figure 4. PexRAP is essential for normal concentrations and distributions of some ether**
965 **phospholipids in splenic follicles.** (A) Schematic of immunization for IMS analyses. Mice of
966 the indicated genotypes were treated with tamoxifen, immunized with SRBC, and harvested 1
967 wk after immunization. (B) Schematic diagram illustrating the 2D-IMS analysis work flow,
968 image merging and quantitation. Harvested spleens were used to generate serial tissue sections
969 followed by immunofluorescence (IF) staining of one section and IMS analysis with the adjacent
970 one. IF and IMS images were aligned to map ion intensity distributions to microanatomic regions
971 (B cell follicle and GC). The intensities of specific ions on B cell follicles and GC regions were
972 quantitated as described in *Materials and Methods.* (C) Identification of ether lipid species
973 localizing to lymphoid follicles. Representative ion images of two ions [*m/z* 752.5545, and *m/z*
974 776.5556] with spleens from immunized mice (WT and *Dhrs7b*$^{\Delta/\Delta}$). (D) Identification of ether
975 lipid species localizing to lymphoid follicles. Representative ion images of three ions [*m/z*
976 752.5545, *m/z* 872.5749, and *m/z* 700.4958] in mass spectrometry imaging of spleens from WT
977 and *Dhrs7b*$^{\Delta/\Delta-B}$ mice. Immunofluorescent images at higher magnification, delineating LZ and
978 DZ marked by CD35 staining, along with quantification of sizes of GC and their LZ and DZ, are
979 shown in supplemental data Fig. S4A, B. (E) Shown in the bar graphs are the mean (±SEM) ion
980 intensities in primary lymphoid follicles (B cell zones) and GC from spleens of WT and
981 *Dhrs7b*$^{\Delta/\Delta-B}$ mice, immunized or not ("UI") as indicated. Median intensity of each ion was
982 obtained from 3 follicles / spleen and 3 GC / spleen from WT and *Dhrs7b*$^{\Delta/\Delta-B}$ mice (three
983 biological replications comprising 7 WT and 6 cKO spleens). P values were calculated by Mann-
984 Whitney U test.
985
986 **Figure 5. B cell intrinsic role of PexRAP in GC response.** (A) Schematic of immunization
987 with NP-OVA in alum after inactivation of *Dhrs7b* in B lineage cells. Tamoxifen-treated WT
988 (*hCD20*-CreER^{T2}; *Dhrs7b*$^{+/+}$) or *Dhrs7b*$^{\Delta/\Delta-B}$ mice *(hCD20*-CreER^{T2}; *Dhrs7b*^{ff}) were immunized
989 with NP-OVA, boosted with NP-OVA 3 wk thereafter, and harvested 1 wk after the 2nd

990 immunization. (B, C) Representative flow plots of splenic IgD^{neg} B cells (B) and aggregate data
991 (C) for two replicate experiments (n = 5 WT and 5 cKO). The cocktail of reagents for the dump
992 channel included anti-IgD. (D, E) B cell-intrinsic function of PexRAP in GC B cell response.
993 Representative flow plots of $GL7^+$ $CD95^+$ GC B cells among viable IgD^{neg} B cells (D), and
994 aggregated frequencies and numbers of GC B cells for two replicate experiments (E). Mann-
995 Whitney U test was used to calculate p values.
996
997 **Figure 6. Ab response and affinity increase promoted by PexRAP in B cells.** Tamoxifen-
998 treated mice (*hCD20*-$CreER^{T2}$; *Dhrs7b*$^{+/+}$ or *hCD20*-$CreER^{T2}$; *Dhrs7b*^{ff} , i.e., *Dhrs7b*$^{\Delta/\Delta-B}$) were
999 immunized as in Fig. 5, with venous blood collected to measure Ag-specific Ab just prior to a
1000 second immunization, followed by harvesting a week thereafter. (A-D) Ag-specific Ab in
1001 primary response sera, prior to the boost. Shown are the all- (NP_{20}) and high- (NP_2) -affinity anti-
1002 NP IgM (A, B) and IgG1 (C, D), as indicated, with NP_{20} a high hapten density to detect both
1003 low- and high-affinity Ab and NP_2 a low hapten density selective for high-affinity Ab.
1004 (E, F) Levels of anti-NP IgM detected using NP_{20} and NP_2 for ELISpot (F) and ELISA (G) as
1005 described in *Materials and Methods*. Graphs show mean (± SEM) number of Ab-secreting cells
1006 in spleen (E) and (F) mean (± SEM) OD_{450nm} in measurement of NP-specific IgM in serial
1007 dilutions of sera. P values were calculated by students' t-test. * indicates $p<0.05$, and **
1008 indicates $p<0.01$. (G) PexRAP regulates Ab affinity maturation. The bar graph shows the mean
1009 (± SEM) ratios of high-affinity to all-affinity NP-specific IgM Ab in sera of individual mice
1010 (each dot representing one subject) using OD_{450nm} values at the 1:2000 dilution, with data from
1011 three independent experiments comprising 8 mice of each type (WT; *Dhrs7b*$^{\Delta/\Delta-B}$). P values were
1012 calculated by Mann-Whitney U test. (H, I) PexRAP promotes $CD138^+$ cell differentiation in
1013 vivo. B cells were adoptively transferred into μMT recipient mice and analyzed at 4 days after
1014 transfer. Representative flow plot of CD138 and cD19 expression (H) and aggregated
1015 frequencies of $CD138^+$ $CD19^+$ cells in the viable cell gate (I) from four independent replicate
1016 experiments. To test for a potential distortion arising from outlier values, statistical testing was
1017 performed both with and without their inclusion.
1018
1019 **Figure 7. Function of PexRAP in GC response.** (A) Schematic of the time line of
1020 immunization followed later by tamoxifen injections into *S1pr2*-$CreER^{T2}$ mice (*Dhrs7b*$^{+/+}$or

1021 *Dhrs7b*$^{f/f}$). Note that deletion is initiated after the germinal center reaction starts (~ 3.5 d post-
1022 immunization). Mice (*S1pr2*-CreER^{T2}; *Dhrs7b*$^{+/+}$ or *S1pr2*-CreER^{T2}; *Dhrs7b*$^{f/f}$) were immunized
1023 with NP-OVA, treated with tamoxifen on days 3, 5, and 7 after NP-OVA immunization (36) and
1024 harvested at day 9. (B) Representative flow plots of GL7^{+} CD95^{+} GC B cells among viable B
1025 cells and (C) aggregated mean (±SEM) frequencies of GC B cells from three replicate
1026 experiments (7 WT; 9 cKO mice). Mann-Whitney U test was used to calculate p values. (D, E)
1027 Effect of PexRAP on the level of plasmablasts in spleen. Representative flow plots of B220^{+}
1028 CD19^{+} plasmablasts among the events in a dump^{-} CD138^{+} TACI^{+} gate (D) and aggregated mean
1029 (±SEM) frequencies of these plasmablasts (E).
1030
1031 **Figure 8. PexRAP contributes to ROS homeostasis and B cell population growth in vitro.**
1032 (A-D) PexRAP is critical for maintenance of normal ROS levels. Bead-purified B cells from
1033 spleens of tamoxifen-treated *huCD20*-CreER^{T2} mice (*Dhrs7b*$^{\Delta/\Delta-B}$ and *Dhrs7b*$^{+/+}$) were cultured
1034 3 days in anti-CD40, BAFF, IL-4, IL-5 and 4-hydroxytamoxifen. Total cellular (A, B) and
1035 mitochondrial ROS, mtROS (C, D) in B lymphoblasts were determined by flow cytometry after
1036 staining with surface markers and H_2DCFDA and MitoSOX, as described in the Methods.
1037 Representative histogram image of H_2DCFDA (A) and MitoSOX (C) in the B cell gate, and
1038 aggregated mean (± SEM) geometric MFI of H_2DCFDA (B) and MitoSOX (D) from 3
1039 independent experiments, each using two mice of each type (6 WT; 6 cKO). P values were
1040 calculated by Mann-Whitney U test. (E) PexRAP restrains lipid peroxidation. B cells were
1041 activated and cultured as in (A). A representative result of flow cytometric analyses of lipid
1042 peroxidation assayed using C11-Bodipy is shown, based on three independent experiments.
1043 (F, G) PexRAP promotes B cell survival. (F) Shown are the mean (±SEM) frequencies of total
1044 viable 'events' (by FSC, SSC, and 7-AAD exclusion) in flow cytometry (filled circles) and MFI
1045 of Bodipy-C11 (open squares) after exposure to H_2O_2 (200 μM). (*, ** - p=0.03 and 0.003,
1046 respectively). (G-I) WT and *Dhrs7b*$^{\Delta/\Delta}$ B cells were cultured (2 d) in anti-CD40, BAFF, IL-4, IL-
1047 5 and 4-hydroxytamoxifen. (G) Increased cleaved caspase 3 (CC3) in PexRAP-deficient cells
1048 generated in vitro. Cleaved caspase 3 in B cells was detected by intracellular staining and flow
1049 cytometry. Shown are a representative pair of histograms for WT and *Dhrs7b*$^{\Delta/\Delta}$ B cells as
1050 indicated (left panel) and a dot graph aggregating all experiments' outcomes (right panel).

1051 (H) Frequencies of apoptotic B cells in cultures as in (A-D) were scored for annexin V and
1052 7AAD as described (84). Shown are representative data of flow plots in the lymphocyte gate
1053 (left panel) and a dot graph aggregating all experiments' outcomes (right panel). (I, J) PexRAP
1054 and ROS control promote B cell population growth in vitro. WT and *Dhrs7b*$^{\Delta/\Delta}$ B cells were
1055 cultured 5 days in anti-CD40, BAFF, IL-4, IL-5 and 4-hydroxytamoxifen in the presence or
1056 absence of ROS scavenger NAC (1 mM vs 5 mM) (H). (I) B cells activated as in (A-G) were
1057 cultured 5 d in the presence or absence of NAC (1 mM) or thioridazine (100 nM). The bar graphs
1058 show the mean (± SEM) recovered cell number from three independent experiments, each with
1059 two independent samples of each genotype (WT; *Dhrs7b*$^{\Delta/\Delta}$).

1060

1061 **Figure 9. PexRAP deficiency in activated B cells reduces mitochondrial metabolism and ER**
1062 **mass.** (A-G) Purified B cells were activated with and cultured (2 d) in αCD40, BAFF, IL-4, IL-5,
1063 and 4-OHT, then divided and analyzed using a Seahorse XFe96. (A) Shown are aggregated
1064 results from three independent experiments measuring oxygen consumption rate (OCR)
1065 quantified via metabolic flux analysis during mitochondrial stress testing. (B) Basal OCR, (C)
1066 maximal OCR, (D) ATP-production coupled respiration, (E) proton leak, and (F) spare
1067 respiratory capacity of WT and *Dhrs7b*$^{\Delta/\Delta}$ B cells assayed in (A). Data points of individual
1068 samples are show (each individual dot), as well as bars to display mean (±SEM) values. T-tests
1069 with Welch's correction were used to calculate p-values. *, $p<0.05$; ***, $p<0.001$. (G)
1070 Extracellular acidification rate (ECAR) of B cells cultured as described previously (36) and
1071 assessed using the glycolytic stress test. (H, I) PexRAP influences ER mass. WT and *Dhrs7b*$^{\Delta/\Delta}$
1072 B cells were cultured 5 days in anti-CD40, BAFF, IL-4, IL-5 and 4-hydroxytamoxifen followed
1073 by the staining with ER-Tracker Green. Representative histogram of ER-Tracker Green in viable
1074 cells (H) and aggregated MFI (±SEM) of ER-Tracker Green from three replicate experiments (I).
1075 Mann-Whitney U test was used to calculate p values.

1076 **SUPPLEMENTAL INFORMATION**

1077

1078 **Supplemental Figures**

1079 **Supplemental Figure 1. PexRAP is dispensable for T cell homeostasis and does not affect**
1080 **balance among pre-immune B cell subsets.** Mice (*Rosa26*-CreER^{T2}; *Dhrs7b*$^{+/+}$*, or Rosa26*-
1081 CreER^{T2}; *Dhrs7b*$^{f/f}$) were treated with tamoxifen and immunized with SRBC as described in
1082 *Materials and Methods,* and 1 wk after immunization. (A-C) PexRAP is dispensable for
1083 homeostatic maintenance of T cells. Shown are the representative flow plots of splenic T cells
1084 (A), mean (± SEM) frequencies of TCRβ^{+} CD4^{+} T cells (B), and CD8 (TCRβ^{+} CD4$^{-)}$ T cells (C)
1085 from WT and cKO mice in three replicate experiments totaling 8 WT and 7 cKO mice. (D) A
1086 representative gating scheme illustrating the flow-cytometric determination of the GC B cell
1087 population in mice. (E) Numbers of GC identified by microscopy of immunofluorescently
1088 stained sections of immunized mice as in Fig. 1. (F) A representative gating scheme illustrating
1089 the flow-cytometric estimation of the MZ, FO, and B1 B cell populations in mice. (G) Shown are
1090 the mean (±SEM) frequencies of CD19^{+} IgM^{+} CD23^{-} MZB cells (left panel) and CD19^{+} IgM^{-}
1091 CD23^{+} FOB cells (righthand panel) in spleen, and (H) CD19^{+} CD23^{lo} CD43^{+} CD5^{+} B1B cells in
1092 peritoneal cavity. (I) In vivo generation of IgD^{-} progeny from four independent replicate
1093 experiments (n =8 WT and 9 cKO). Shown are mean (±SEM) frequencies of IgD^{-} B cells as
1094 aggregate data for the frequencies of IgD- events in the gate for viable B cells recovered from
1095 μMT recipient mice after transfer of WT or PexRAP-depleted B cells (experiments of Fig. 2D-
1096 F), as indicated, with representative flow plots in Fig. 2E.

1097

1098 **Supplemental Figure 2. Activation of B cells induces PexRAP-dependent increases in their**
1099 **ether and plasmalogen P-lipids.** As in Fig. 3, B lymphocytes of the indicated *Dhrs7b* genotypes
1100 were prepared from individual tamoxifen-injected mice and divided to analyze without activation
1101 ("naive") or after activation and culture (48 h) ("activated"). Shown are heat maps with more
1102 extensive lists of ether phospholipids and plasmalogens identified in the LC-MS-MS analyses for
1103 both genotypes in positive (A) and negative (B) ion modes. (C, D) LC-MS-MS results for lipids
1104 in B cells, activated or not, as indicated, of conventional non-transgenic B6 mice not injected
1105 with tamoxifen and those of tamoxifen-injected CreER^{T2+} mice (the "+/+" samples of panels A,
1106 B and of Figure 3). Bar graphs in (C) and (D) show results of these control comparisons for some
1107 of the phospholipids analyzed in prior figures panels (Fig. 3A, B).

1108 **Supplemental Figure 3. Immunization induces increases in P-lipids of both primary and**
1109 **secondary follicles dependent on PexRAP in B cells.** (A, B) Selected representative *m/z*
1110 features Spleens of AID-GFP were harvested at 7 days after immunization with SRBC and
1111 analyzed for exact mass signatures of ether lipid species in (A) negative and (B) positive ion
1112 modes. (C) Spleens of immunized mice (tamoxifen-treated *hCD20*-CreER^{T2}; *Dhrs7b$^{f/f}$* and
1113 *hCD20*-CreER^{T2} controls) were analyzed by IMS. Shown are the positive ions presented in (B)
1114 for GC vs follicles of immunized AID-GFP mice. The bar graph shows the mean (± SEM) ion
1115 intensities in lymphoid follicles and GC from WT and *Dhrs7b$^{\Delta/\Delta-B}$* spleens. Median intensity of
1116 each ion was obtained from three follicles per spleen and three GC per spleen from WT and
1117 *Dhrs7b$^{\Delta/\Delta-B}$* mice (three biological replication experiments totaling seven WT and six cKO
1118 subjects). P values were calculated by Mann-Whitney U test.
1119
1120 **Supplemental Figure 4. A subset of ether phospholipids in primary follicles and GC**
1121 **(secondary follicles) depend on PexRAP in B cells.** (A) As in Fig. 4, *Dhrs7b* was inactivated
1122 by tamoxifen injections into mice bearing the hCD20-CreER^{T2} transgene, followed by
1123 immunization with SRBC and analysis. Shown are representative higher-magnification images
1124 defining the primary (IgD^{+}) and secondary (IgD$^{lo/neg}$, GL7^{+}) follicles and the identification of
1125 light (CD35^{+}) and dark (CD35^{neg}) zones. (B) The sizes of GC and their light zones (LZ) after
1126 immunization were quantified. Spleens of immunized mice (tamoxifen-treated *hCD20*-CreER^{T2};
1127 *Dhrs7b$^{f/f}$* and *hCD20*-CreER^{T2} controls, as indicated) were analyzed by immunofluorescence
1128 staining as in (A). Each dot represents one follicle in a given mouse. Totals of three GC per
1129 spleen from immunized mice were used were used, with seven WT and five *Dhrs7b$^{\Delta/\Delta-B}$*.
1130 (C, D) Mean (±SEM) absorbances of ELISA performed across the indicated dilutions of sera
1131 from the tamoxifen-treated mice (*hCD20*-CreER^{T2}; *Dhrs7b$^{+/+}$* or *hCD20*-CreER^{T2}; *Dhrs7b$^{f/f}$* ,
1132 i.e., *Dhrs7b$^{\Delta/\Delta-B}$*) of Fig. 6. Shown are the results for (C) all- (NP_{20} captured) and (D) high- (NP_2
1133 captured) -affinity anti-NP Ab of the IgG1 and IgG2c isotypes, as indicated. (E) Proliferation and
1134 development of CD138^{+} progeny. Shown are representative flow plots from three independent
1135 experiments with six WT and seven *Dhrs7b$^{\Delta/\Delta-B}$* mice.
1136
1137 **Supplemental Figure 5. Distinct outcomes of heightened ROS elicited by H_2O_2 versus**
1138 **menadione.** (A-B) Induction of ROS independent from B cell activation. Shown are
1139 representative flow plots of DCFDA in the viable B cell gate after exposure (1 h) (A) to H_2O_2

1140 (200 μM) or (B) menadione (8 μM), as in (87). (C-D) Representative flow plots of annexin V vs
1141 7-AAD for identification of early-apoptotic B cells. Cultured B cells were analyzed 3 hr after
1142 treatment with (C) 200 μM H_2O_2 or (D) 8 μM menadione. Inset numbers represent the fraction
1143 of B cells that are Annexin V^+ 7-AAD^{neg} or Annexin V^{neg} 7-AAD^+. (E-G) Shown are the results
1144 of three independent experiments to measure (E) total cell viability, (F) BODIPY C11 MFI and
1145 (G) frequencies of Annexin V^+ 7-AAD^{neg} frequency in B cells treated (8 μM) menadione
1146 overnight (E) or for 3 h (D). P-values were calculated using the unpaired Student's t-test.
1147
1148
1149 **Supplemental Table 1. Immunization-induced increases of selected ether lipids in GC.**
1150 Shown are (a) a sample of *m/z* features characteristic of the indicated phospholipid species
1151 identified by the LIPIDMAPS database, and (b) the mean ±SEM ion intensity / counts in IMS
1152 data generated from spleens of AID-GFP mice, immunized or not (UI), after mapping to the
1153 indicated regions of interest (primary follicles or GC, i.e. secondary follicles) using fluorescent
1154 images. Shown are ions more accumulated in GC regions compared to primary follicles (8 ions
1155 from negative ion mode, and 5 ions from positive ion mode, all $p<0.05$ for comparison of 1^0
1156 follicle to UI (c), or GC to 1^0 follicle (d). P values were calculated by Mann-Whitney U test.
1157
1158 **Supplemental Table 2. . Impact of PexRAP on relative quantities of selected lipid species in**
1159 **primary and secondary follicles (GC).** As in Table 1 except that B cells of immunized mice
1160 were either WT or lacked PexRAP (cKO, i.e., *Dhrs7b*$^{\Delta/\Delta\text{-B}}$). Shown are (a) a sample
1161 of *m/z* features characteristic of the indicated phospholipid species. (b) the mean ±SEM ion
1162 intensity counts in IMS data after mapping to the indicated regions of interest as in Table 1. (c-f)
1163 indicate that $p<0.05$ for the null hypothesis in considering a difference between WT mouse
1164 spleens after immunization versus UI controls (c), 1^0 B cell follicles in spleens of immunized
1165 WT vs *Dhrs7b*$^{\Delta/\Delta\text{-B}}$ mice (d), GC vs in 1^0 B cell follicles in spleens of immunized WT mice (e),
1166 and GC of immunized WT vs *Dhrs7b*$^{\Delta/\Delta\text{-B}}$ mice (f) in the ions counts for designated *m/z* features.
1167 P values were calculated by Mann-Whitney U test.

Table 1.

Immunization-induced increases of selected lipids in GC

Negative Ions			
m/z [a] **Lipid ID**	**UI**	**1° B cell Follicle**	**GC**
716.5216 PE(18:0_16:1)	618 ± 22 [b]	2400 ± 83 [c]	3674 ± 154 [d]
752.5545 PE(O-18:0_20:4)	301 ± 14	1739 ± 33 [c]	1960 ± 52 [d]
760.5056 PE(16:0_22:6)	203 ± 4	1816 ± 30 [c]	2031 ± 23 [d]
772.5242 PE(P-18:1_22:6)	234 ± 5	2334 ± 47 [c]	2578 ± 63 [d]
776.5556 PE(O-18:0_22:6)	277 ± 9	1638 ± 51 [c]	2074 ± 90 [d]
869.5526 PI(O-18:0_20:5)	242 ± 7	1611 ± 24 [c]	1789 ± 15 [d]
872.576 PC(18:0_24:0)	171 ± 6	1167 ± 16 [c]	1369 ± 18 [d]
888.5612 PS(22:1_22:6)	506 ± 13	2684 ± 54 [c]	3386 ± 72 [d]

Positive Ions			
m/z [a] **Lipid ID**	**UI**	**1° B cell Follicle**	**GC**
739.4587 PG(12:0_20:3)	3042 ± 102	3733 ± 116 [c]	4778 ± 274 [d]
740.465 PC(16:0_15:1)	1310 ± 13	1478 ± 66 [c]	1933 ± 142 [d]
784.5564 PC(10:0_24:0)	2840 ± 24	7956 ± 147 [c]	9856 ± 270 [d]
798.5347 PC(10:0_25:0)	9937 ± 269	27589 ± 574 [c]	34733 ± 1644 [d]
799.5375 PG(18:0_18:1)	5665 ± 65	12078 ± 282 [c]	15311 ± 790 [d]

Table 2. Impact of PexRAP on relative quantities of selected lipid species in primary and secondary follicles (GC).

Negative Ions					
m/z [a] Lipid ID	**UI**	**WT follicle**	**PexRap cKO follicle**	**WT GC**	**PexRap cKO GC**
436.2801 LPE (O-16:1)	315 ± 4	369 ± 7	374 ± 11	610 ± 20 [e]	475 ± 19
716.5216 PE (18:0_16:1)	754 ± 43 [b]	1608 ± 182 [c]	1263 ± 112	2729 ± 247 [e]	1770 ± 137 [f]
746.5098 PE (O-16:1_22:6)	622 ± 19	672 ± 35	609 ± 23	1066 ± 39 [e]	836 ± 39
752.5545 PE (O-18:0_20:4)	459 ± 49	657 ± 51 [c]	548 ± 46 [d]	1191 ± 61 [e]	734 ± 25 [f]
760.5056 PE (16:0_22:6)	229 ± 8	386 ± 25 [c]	312 ± 16 [d]	569 ± 27 [e]	408 ± 15 [f]
772.5242 PE (P-18:1_22:6)	388 ± 47	617 ± 46 [c]	499 ± 33 [d]	918 ± 21 [e]	646 ± 9 [f]
776.5556 PE (O-18:0_22:6)	449 ± 53	661 ± 50 [c]	562 ± 46	1130 ± 49 [e]	789 ± 13 [f]
869.5526 PI (O-18:0_20:5)	509 ± 81	641 ± 50 [c]	494 ± 40 [d]	1014 ± 21 [e]	690 ± 12 [f]
872.576 PC (18:0_24:0)	230 ± 19	285 ± 12 [c]	247 ± 9 [d]	522 ± 17 [e]	336 ± 9 [f]
888.5612 PS (22:1_22:6)	1423 ± 277	2051 ± 199 [c]	1904 ± 199	3260 ± 156 [e]	2629 ± 80 [f]

Positive Ions					
m/z [a] Lipid ID	**UI**	**WT follicle**	**PexRap cKO follicle**	**WT GC**	**PexRap cKO GC**
730.5767 PE (P-18:0_18:1)	91 ± 3	97 ± 3	85 ± 3	130 ± 7 [e]	102 ± 4
739.4587 PG (12:0_20:3)	3042 ± 102	3094 ± 40	2944 ± 31 [d]	3506 ± 140 [e]	3011 ± 46 [f]
784.5564 PC (10:0_24:0)	2840 ± 24	2917 ± 74	2617 ± 46 [d]	3522 ± 102 [e]	2561 ± 42 [f]
798.5347 PC (10:0_25:0)	9937 ± 269	10928 ± 214[c]	11372 ± 155 [d]	15378 ± 116 [e]	14694 ± 186 [f]
801.5509 PG (18:0_18:0)	1540 ± 37	1591 ± 46	1633 ± 26	1444 ± 27 [e]	1533 ± 22 [f]
847.5361 PI (15:0_18:0)	1277 ± 24	1339 ± 54	1217 ± 35	1150 ± 46 [e]	1044 ±44
874.5623 PC (20:5_22:6)	754 ± 39	688 ± 48	675 ± 25	469 ± 27 [e]	556 ± 37

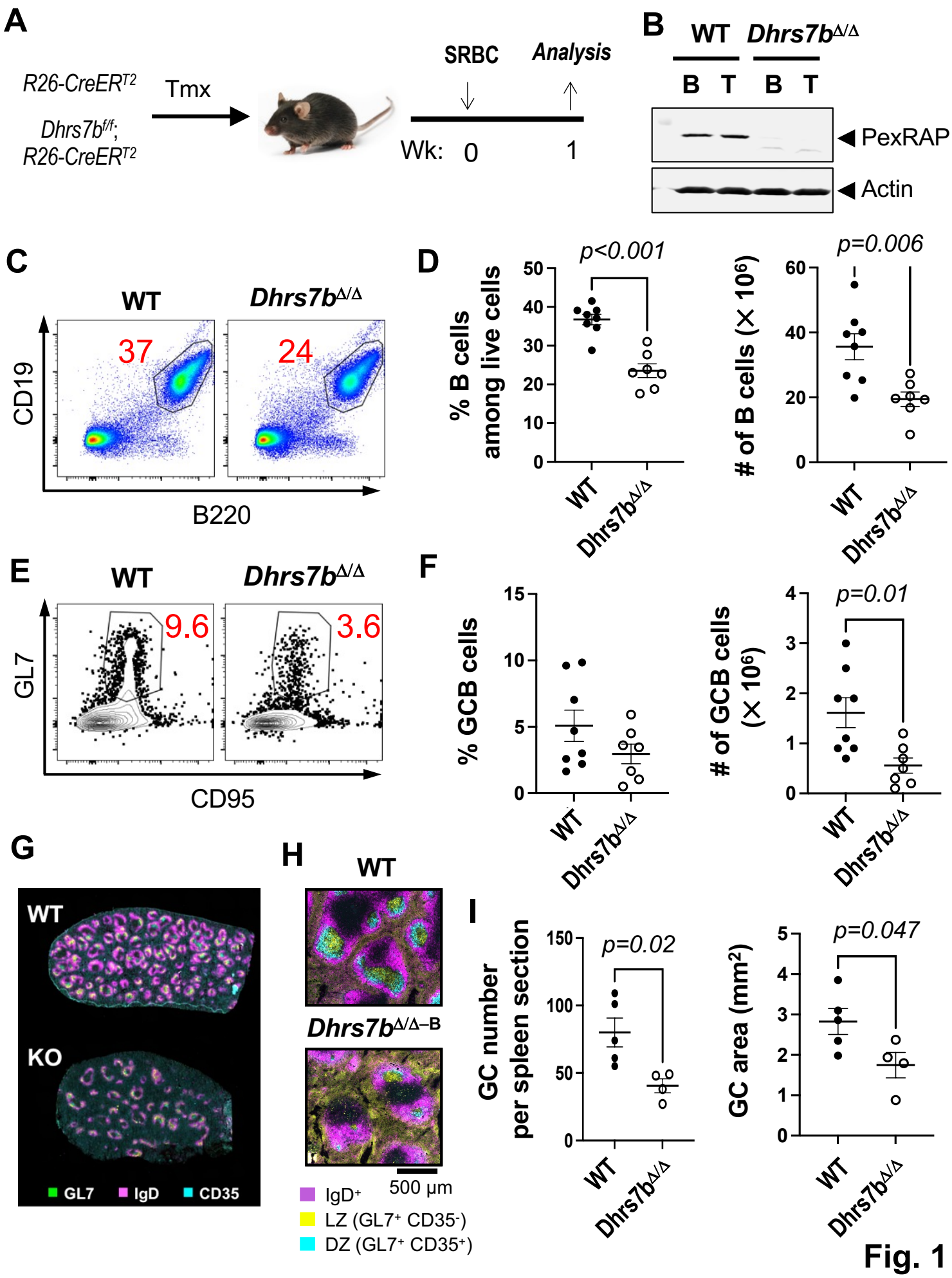
A
R26-CreERT2
Dhrs7bf/f;
R26-CreERT2
Tmx
SRBC
Analysis
Wk: 0
1
B
WT
Dhrs7bΔ/Δ
B T B T
PexRAP
Actin
C
WT
Dhrs7bΔ/Δ
37
24
CD19
B220
D
p<0.001
% B cells among live cells
p=0.006
# of B cells (× 10^6)
WT
Dhrs7bΔ/Δ
E
WT
Dhrs7bΔ/Δ
9.6
3.6
GL7
CD95
F
% GCB cells
p=0.01
# of GCB cells (× 10^6)
WT
Dhrs7bΔ/Δ
G
WT
KO
GL7
IgD
CD35
H
WT
Dhrs7bΔ/Δ–B
500 μm
IgD+
LZ (GL7+ CD35-)
DZ (GL7+ CD35+)
I
GC number per spleen section
p=0.02
GC area (mm2)
p=0.047
WT
Dhrs7bΔ/Δ

Fig. 1

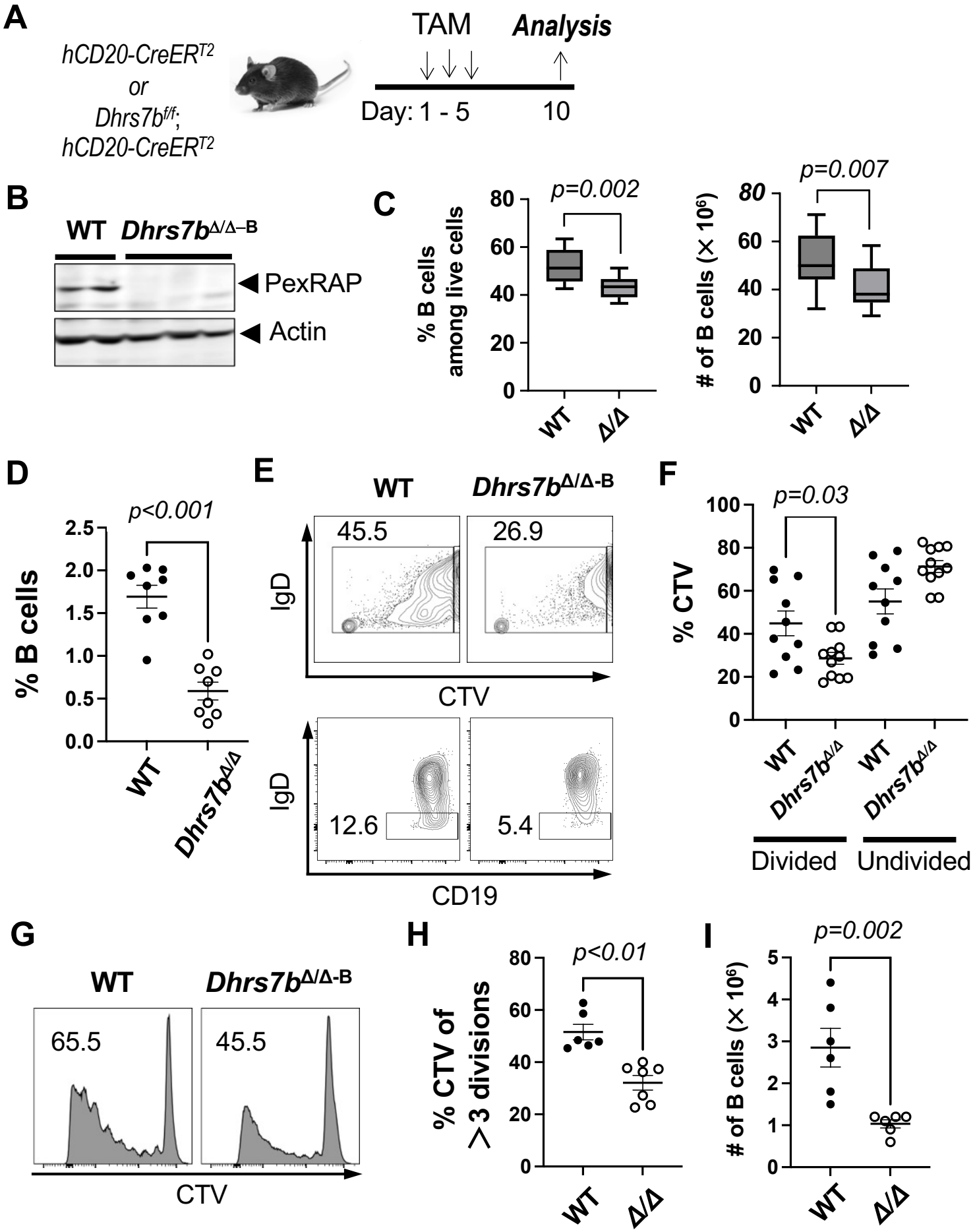
A
hCD20-CreERT2
or
Dhrs7bf/f;
hCD20-CreERT2
TAM
Analysis
Day: 1 - 5
10
B
WT
Dhrs7bΔ/Δ–B
PexRAP
Actin
C
p=0.002
% B cells among live cells
WT
Δ/Δ
p=0.007
# of B cells (× 10^6)
D
p<0.001
% B cells
WT
Dhrs7bΔ/Δ
E
WT
Dhrs7bΔ/Δ-B
45.5
26.9
IgD
CTV
12.6
5.4
CD19
F
p=0.03
% CTV
Divided
Undivided
G
65.5
45.5
CTV
H
p<0.01
% CTV of >3 divisions
I
p=0.002
# of B cells (× 10^6)

Fig. 2

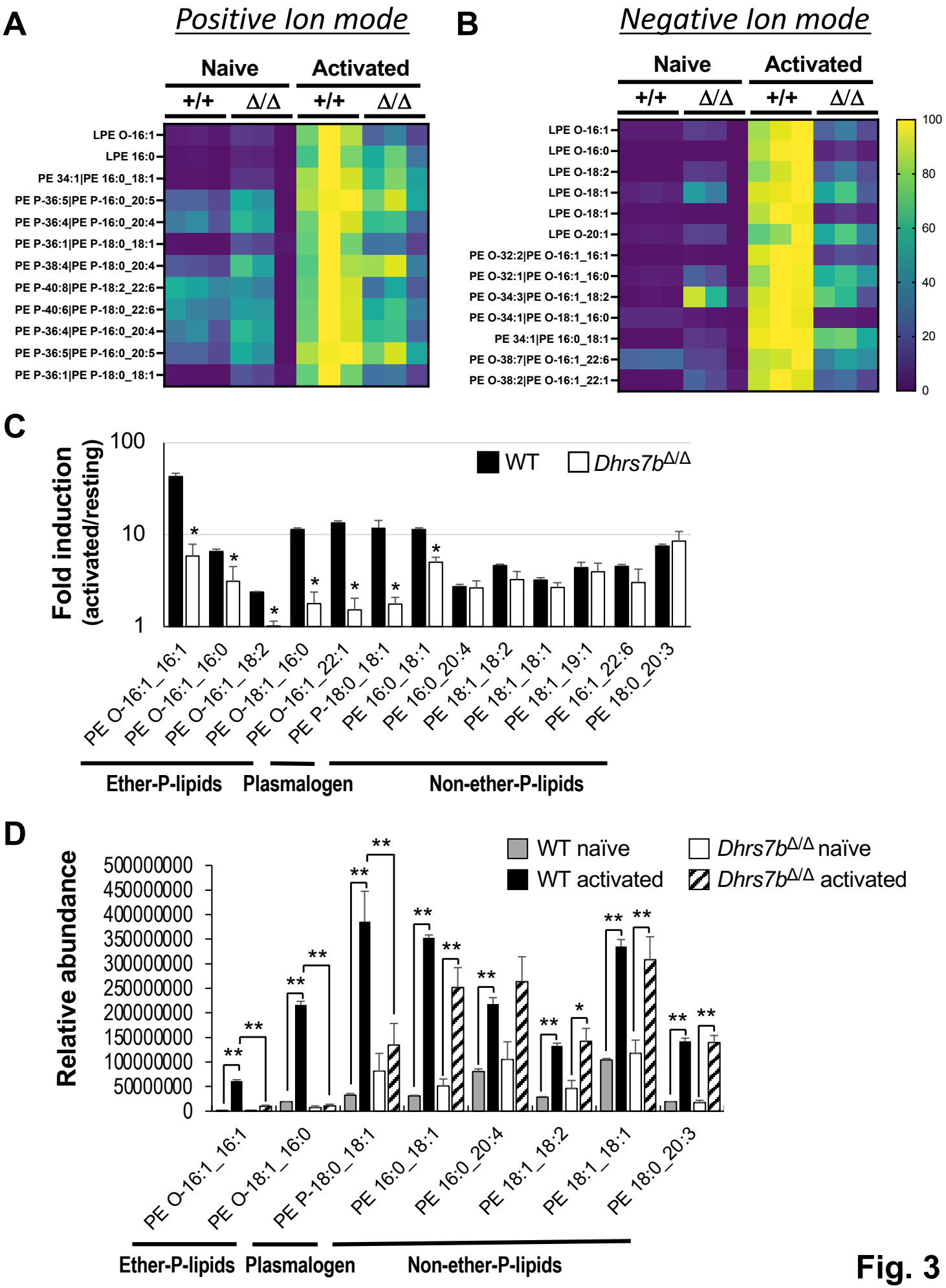
A
Positive Ion mode
Naive
Activated
+/+
Δ/Δ
+/+
Δ/Δ
LPE O-16:1
LPE 16:0
PE 34:1|PE 16:0_18:1
PE P-36:5|PE P-16:0_20:5
PE P-36:4|PE P-16:0_20:4
PE P-36:1|PE P-18:0_18:1
PE P-38:4|PE P-18:0_20:4
PE P-40:8|PE P-18:2_22:6
PE P-40:6|PE P-18:0_22:6
PE P-36:4|PE P-16:0_20:4
PE P-36:5|PE P-16:0_20:5
PE P-36:1|PE P-18:0_18:1
B
Negative Ion mode
Naive
Activated
+/+
Δ/Δ
+/+
Δ/Δ
LPE O-16:1
LPE O-16:0
LPE O-18:2
LPE O-18:1
LPE O-18:1
LPE O-20:1
PE O-32:2|PE O-16:1_16:1
PE O-32:1|PE O-16:1_16:0
PE O-34:3|PE O-16:1_18:2
PE O-34:1|PE O-18:1_16:0
PE 34:1|PE 16:0_18:1
PE O-38:7|PE O-16:1_22:6
PE O-38:2|PE O-16:1_22:1
100
80
60
40
20
0
C
Fold induction
(activated/resting)
100
10
1
WT
Dhrs7b Δ/Δ
PE O-16:1_16:1
PE O-16:1_16:0
PE O-16:1_18:2
PE O-18:1_16:0
PE O-16:1_22:1
PE P-18:0_18:1
PE 16:0_18:1
PE 16:0_20:4
PE 18:1_18:2
PE 18:1_18:1
PE 18:1_19:1
PE 16:1_22:6
PE 18:0_20:3
Ether-P-lipids
Plasmalogen
Non-ether-P-lipids
D
Relative abundance
500000000
450000000
400000000
350000000
300000000
250000000
200000000
150000000
100000000
50000000
0
WT naïve
WT activated
Dhrs7b Δ/Δ naïve
Dhrs7b Δ/Δ activated
PE O-16:1_16:1
PE O-18:1_16:0
PE P-18:0_18:1
PE 16:0_18:1
PE 16:0_20:4
PE 18:1_18:2
PE 18:1_18:1
PE 18:0_20:3
Ether-P-lipids
Plasmalogen
Non-ether-P-lipids

Fig. 3

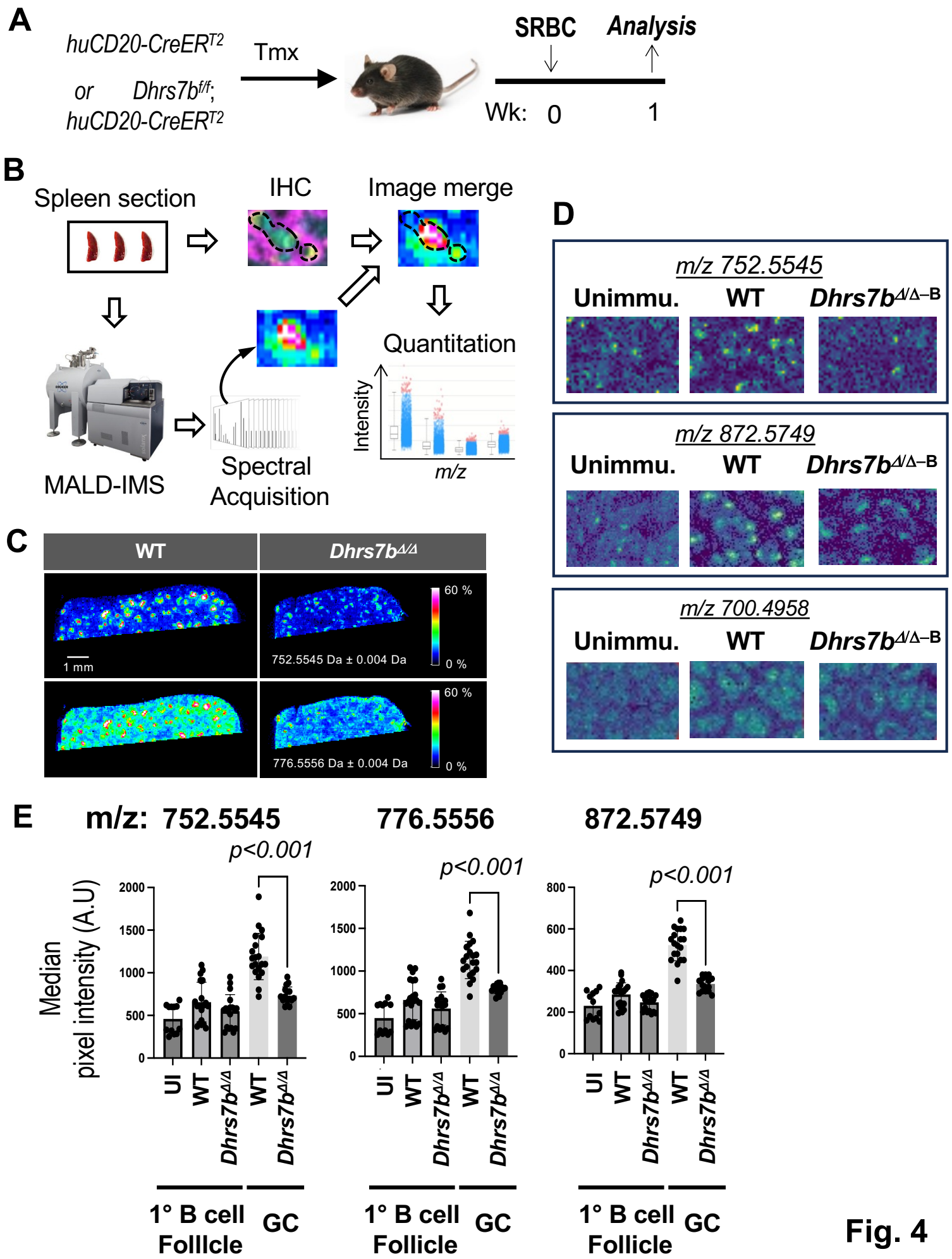
A
huCD20-CreERT2
or Dhrs7b f/f;
huCD20-CreERT2
Tmx
SRBC
Analysis
Wk: 0
1
B
Spleen section
IHC
Image merge
Quantitation
Intensity
m/z
MALD-IMS
Spectral
Acquisition
C
WT
Dhrs7bΔ/Δ
60 %
0 %
1 mm
752.5545 Da ± 0.004 Da
776.5556 Da ± 0.004 Da
D
m/z 752.5545
m/z 872.5749
m/z 700.4958
Unimmu.
WT
Dhrs7bΔ/Δ–B
E
m/z: 752.5545
776.5556
872.5749
p<0.001
Median
pixel intensity (A.U)
UI
WT
Dhrs7bΔ/Δ
1° B cell
Folllcle
Follicle
GC

Fig. 4

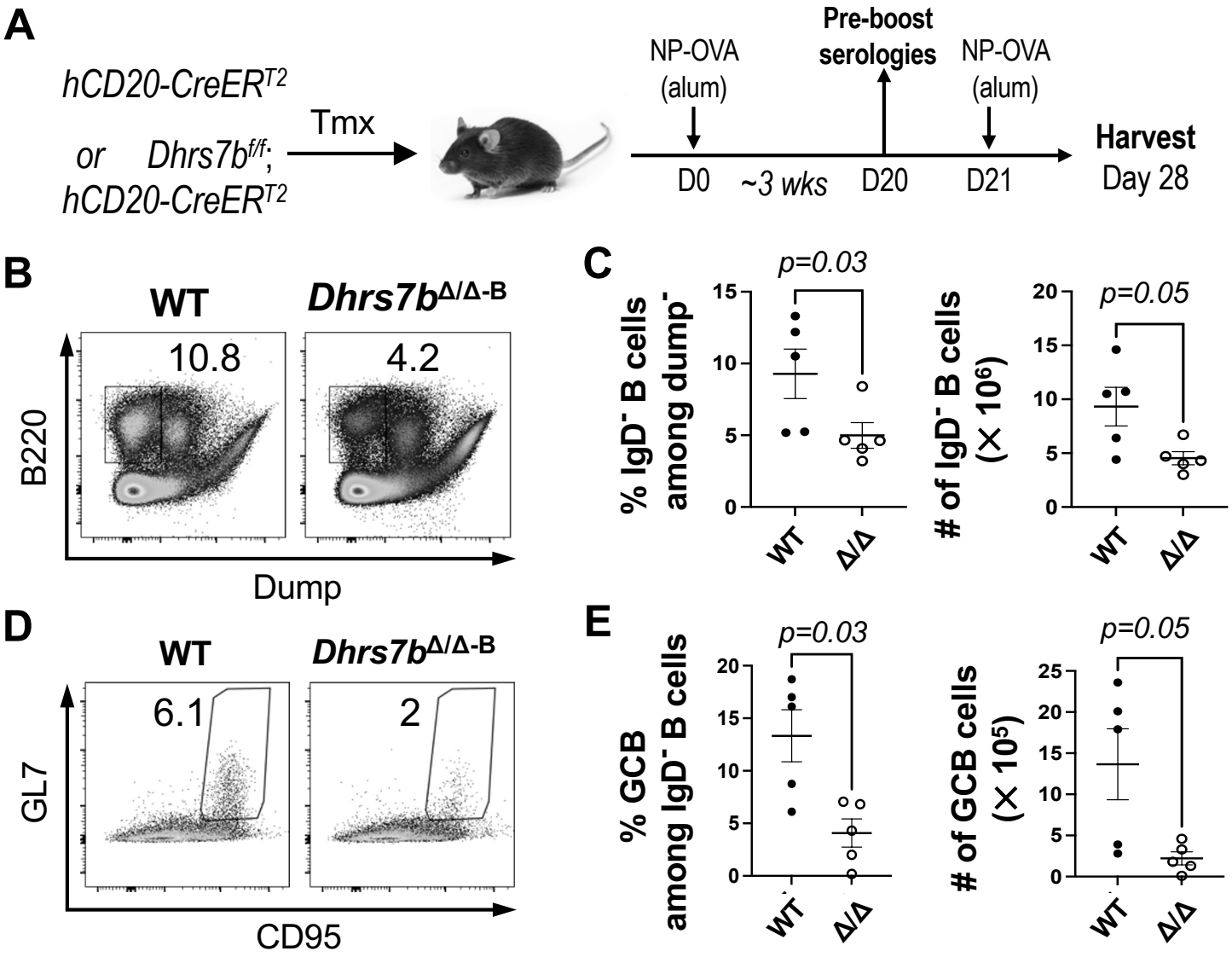
A
hCD20-CreERT2
or Dhrs7bf/f;
hCD20-CreERT2
Tmx
NP-OVA
(alum)
Pre-boost
serologies
NP-OVA
(alum)
Harvest
Day 28
D0
~3 wks
D20
D21
B
WT
Dhrs7bΔ/Δ-B
10.8
4.2
B220
Dump
C
p=0.03
% IgD- B cells
among dump-
p=0.05
# of IgD- B cells
(× 10^6)
WT
Δ/Δ
D
WT
Dhrs7bΔ/Δ-B
6.1
2
GL7
CD95
E
p=0.03
% GCB
among IgD- B cells
p=0.05
# of GCB cells
(× 10^5)
WT
Δ/Δ

Fig. 5

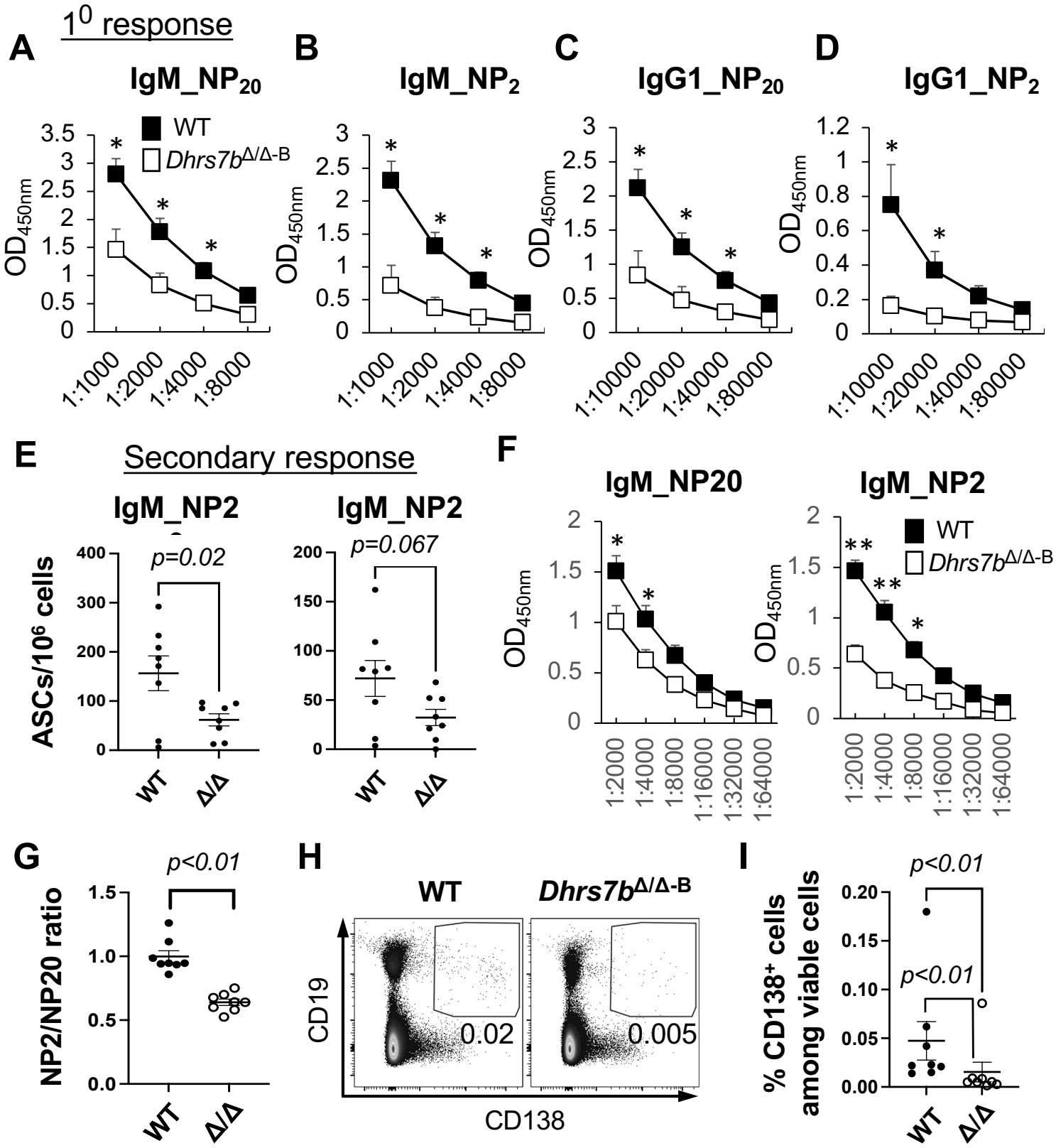
1⁰ response
A
IgM_NP20
WT
Dhrs7bΔ/Δ-B
OD450nm
1:1000
1:2000
1:4000
1:8000
B
IgM_NP2
C
IgG1_NP20
1:10000
1:20000
1:40000
1:80000
D
IgG1_NP2
E
Secondary response
IgM_NP2
ASCs/10⁶ cells
p=0.02
p=0.067
WT
Δ/Δ
F
IgM_NP20
IgM_NP2
1:2000
1:4000
1:8000
1:16000
1:32000
1:64000
G
NP2/NP20 ratio
p<0.01
H
WT
Dhrs7bΔ/Δ-B
CD19
CD138
0.02
0.005
I
% CD138⁺ cells among viable cells
p<0.01

Fig. 6

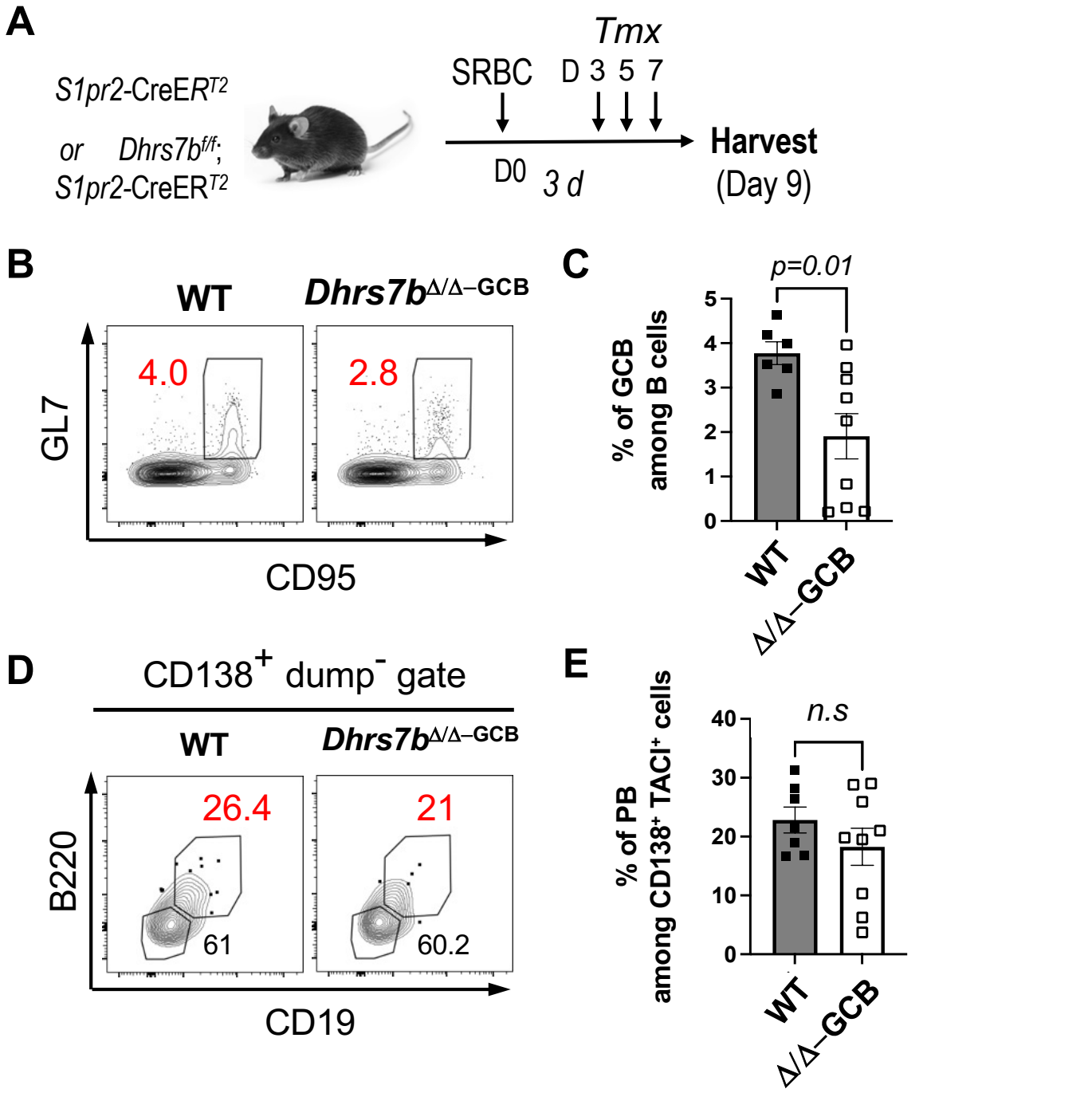
A
S1pr2-CreERT2
or Dhrs7bf/f;
S1pr2-CreERT2
Tmx
SRBC
D 3 5 7
D0
3 d
Harvest
(Day 9)
B
WT
Dhrs7bΔ/Δ–GCB
4.0
2.8
GL7
CD95
C
p=0.01
% of GCB
among B cells
WT
Δ/Δ–GCB
D
CD138+ dump- gate
WT
Dhrs7bΔ/Δ–GCB
26.4
21
61
60.2
B220
CD19
E
n.s
% of PB
among CD138+ TACI+ cells
WT
Δ/Δ–GCB

Fig. 7

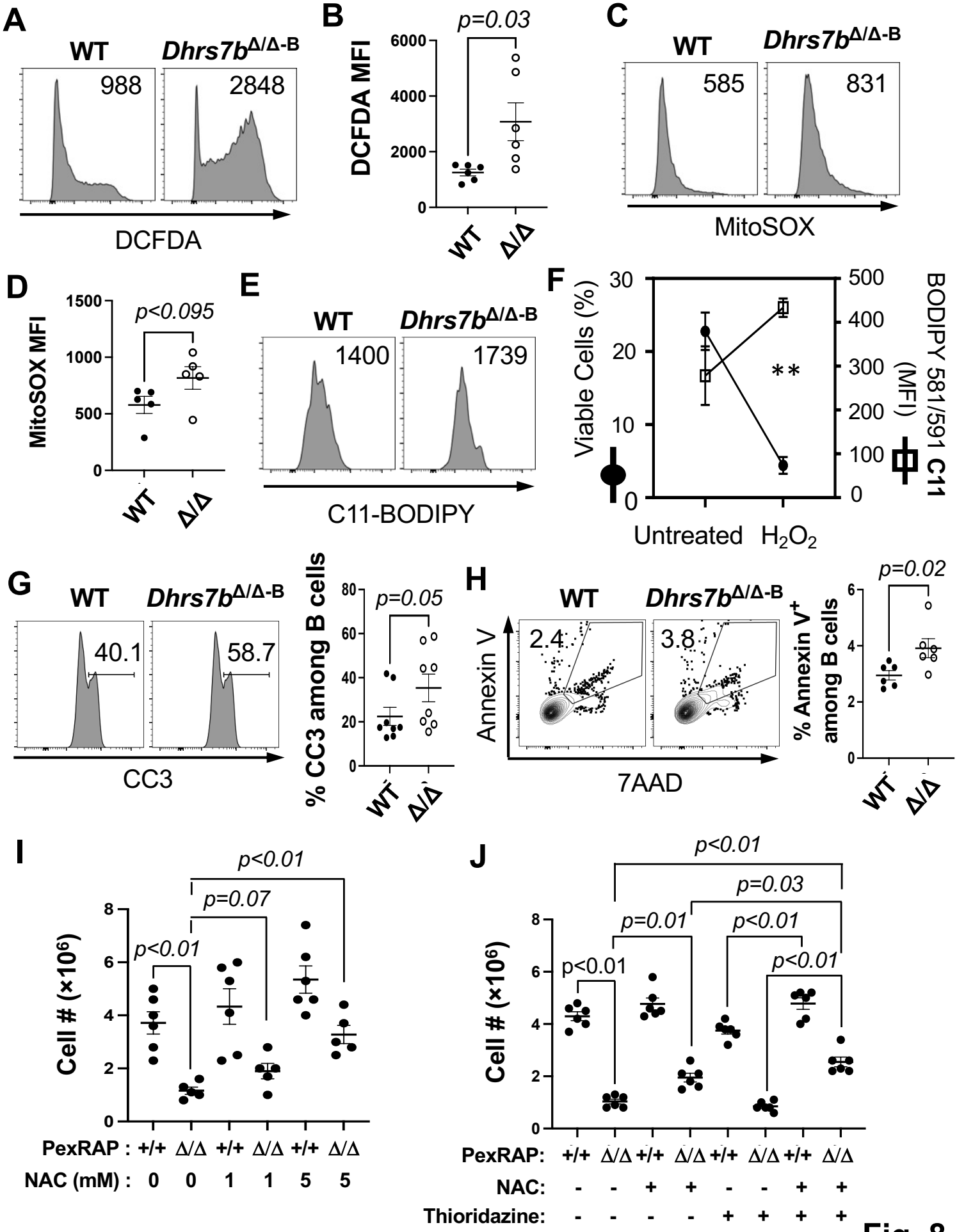
A
WT
Dhrs7b Δ/Δ-B
988
2848
DCFDA
B
p=0.03
DCFDA MFI
6000
4000
2000
0
WT
Δ/Δ
C
WT
Dhrs7b Δ/Δ-B
585
831
MitoSOX
D
MitoSOX MFI
1500
1000
500
0
p<0.095
WT
Δ/Δ
E
WT
Dhrs7b Δ/Δ-B
1400
1739
C11-BODIPY
F
Viable Cells (%)
30
20
10
0
**
BODIPY 581/591 C11 (MFI)
500
400
300
200
100
0
Untreated
H2O2
G
WT
Dhrs7b Δ/Δ-B
40.1
58.7
CC3
% CC3 among B cells
80
60
40
20
0
p=0.05
WT
Δ/Δ
H
WT
Dhrs7b Δ/Δ-B
Annexin V
2.4
3.8
7AAD
% Annexin V+ among B cells
6
4
2
0
p=0.02
WT
Δ/Δ
I
Cell # (×10^6)
8
6
4
2
0
p<0.01
p=0.07
p<0.01
PexRAP : +/+ Δ/Δ +/+ Δ/Δ +/+ Δ/Δ
NAC (mM) : 0 0 1 1 5 5
J
Cell # (×10^6)
8
6
4
2
0
p<0.01
p=0.03
p=0.01
p<0.01
p<0.01
p<0.01
PexRAP: +/+ Δ/Δ +/+ Δ/Δ +/+ Δ/Δ +/+ Δ/Δ
NAC: - - + + - - + +
Thioridazine: - - - - + + + +

Fig. 8

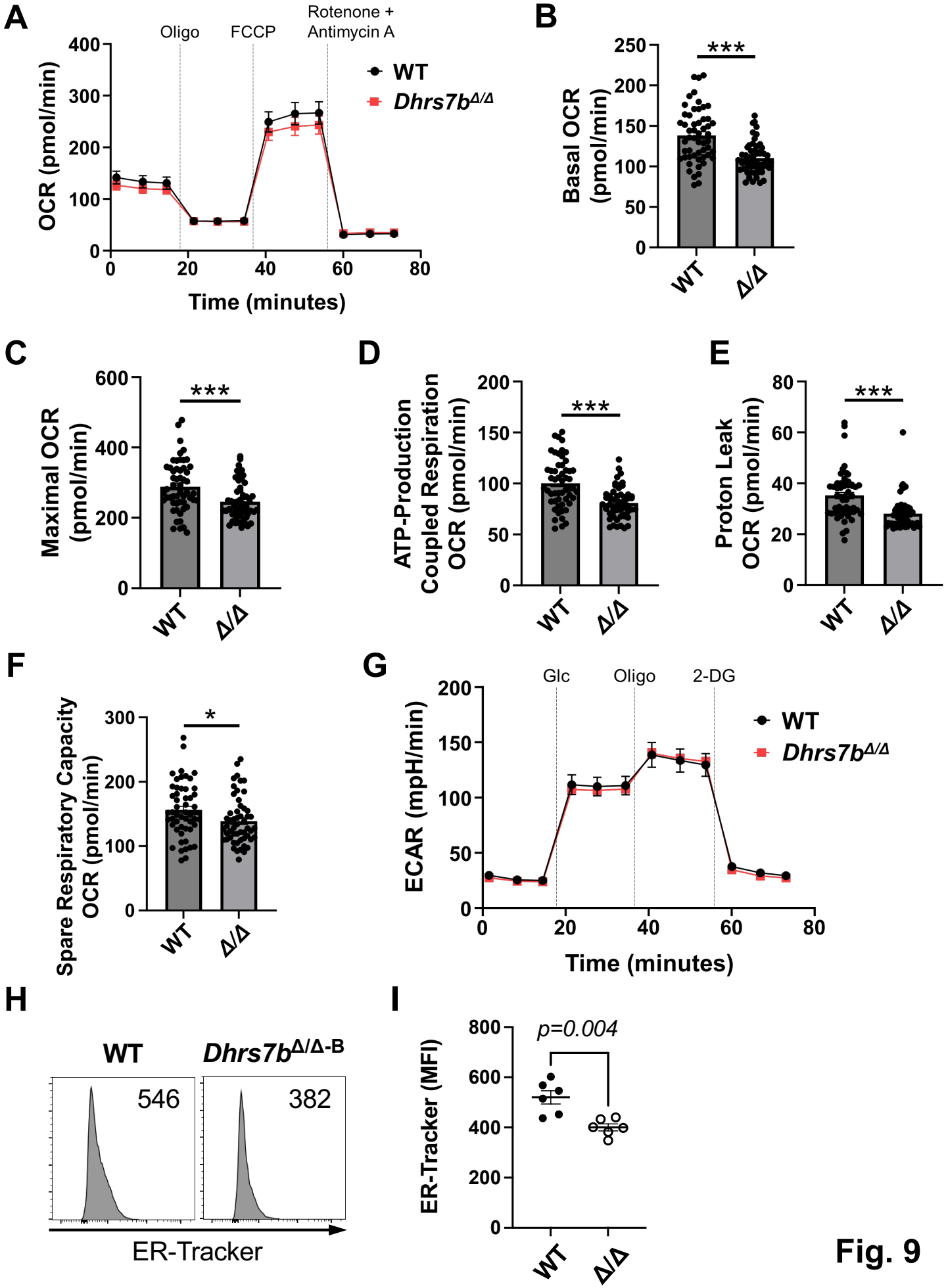
A
Oligo
FCCP
Rotenone +
Antimycin A
WT
Dhrs7bΔ/Δ
OCR (pmol/min)
Time (minutes)
B
Basal OCR
(pmol/min)
***
WT
Δ/Δ
C
Maximal OCR
(pmol/min)
***
D
ATP-Production
Coupled Respiration
OCR (pmol/min)
***
E
Proton Leak
OCR (pmol/min)
***
F
Spare Respiratory Capacity
OCR (pmol/min)
*
G
Glc
Oligo
2-DG
ECAR (mpH/min)
Time (minutes)
H
WT
Dhrs7bΔ/Δ-B
546
382
ER-Tracker
I
p=0.004
ER-Tracker (MFI)

Fig. 9